EVALUATION OF THE PLUMB LINE CURVATURE EFFECT ON THE DEFLECTION OF THE VERTICAL

HUNG PEN-SHAN

January 1986

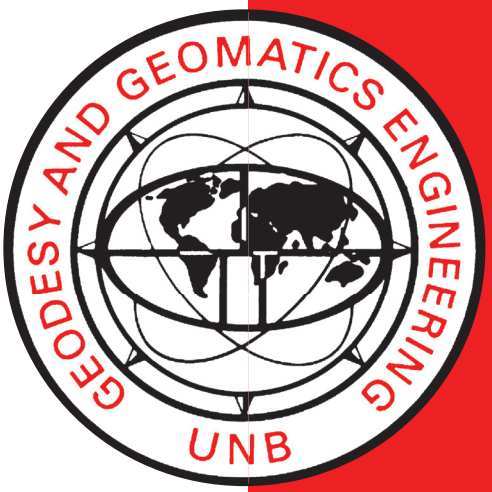

TECHNICAL REPORT
NO. 121

PREFACE

In order to make our extensive series of technical reports more readily available, we have scanned the old master copies and produced electronic versions in Portable Document Format. The quality of the images varies depending on the quality of the originals. The images have not been converted to searchable text.

EVALUATION OF THE PLUMB LINE CURVATURE EFFECT ON THE DEFLECTIONS OF THE VERTICAL

Hung Pen-shan

This report is an unaltered printing of the author's
Master of Science in Engineering thesis
submitted to this department in
October 1985

Department of Geodesy and Geomatics Engineering
University of New Brunswick
P.O. Box 4400
Fredericton, N.B.
Canada
E3B 5A3

January 1986
Latest Reprinting February 1994

ABSTRACT

The curvature of the plumb line should be considered in order to find the undistorted geodetic networks without the plumb line curvature effect and to determine the astro-geodetic geoid as well as for other purposes. A few approaches have been developed to estimate the curvature effect. In most of the methods, the need for sufficient gravity data, the knowledge of the density distribution, and other data make the estimation of the plumb line curvature effect a difficult task.

Without knowing the density distribution inside the earth, the curvature effect can be determined from the use of Vening Meinesz's and Molodenskij's formulae together. However, the procedure is laborious and time-consuming, and the integrations should be extended over the whole earth.

This thesis investigates the utilization of the combination of Stokes's and Molodenskij's approaches to determine the curvature effect of the plumb line. In other words, the determination of the curvature effect of the plumb line is based on combining Vening Meinesz's and Molodenskij's formulae. In this approach, the integrations will not be extended over the whole earth but a 25x25 minutes rectangular area.

A determination of the plumb line curvature effect has been attempted at six stations in New Brunswick. The results show that this approach has been successfully used and can give a higher accuracy. The estimation of the curvature effect of the plumb line is no longer a difficult job.

ACKNOWLEDGEMENTS

I would like to express sincere gratitude to my supervisor, Dr. Petr Vaníček for his patient guidance and encouragement. His rigorous and detailed criticism of the manuscript has been of great profit to me.

I would also like to express thanks to the Geodesy Group for their suggestions and comments on this work and particularly to my friend Hassan Fashir, who took a lot of time to discuss with me. I am indebted to Dr. Carol Morrell for her help in improving the English of the manuscript.

Last but not least, I express special thanks to my family for their distant encouragement and sincere thanks to my Government of the Republic of China for giving me this opportunity.

TABLE OF CONTENTS

LIST OF TABLES

LIST OF FIGURES

CHAPTER 1

INTRODUCTION

The utilization of the concepts of gravity and its potential in geodesy can be classified into two groups: the operation with the magnitude of gravity in the gravimetric methods and the use of the direction of the gravity vector in the astro-geodetic methods. The gravity vector at any point is tangential to the plumb line at that point. Because of the irregular density distribution of the earth, the plumb line is not a straight line but a curve. Therefore, the astronomic observations made on the surface of the earth are not identical to their corresponding values on the geoid. The discrepancies arise from the effect the curvature of the plumb line. In order to make these quantities comparable, the correction of the curvature effect of the plumb line must be taken into account.

For the determination of the geoid by means of the astro-geodetic mehtod, the astro-geodetic deflections (or surface deflections) must be reduced downward to the geoid. This reduction is achieved by taking into account the curvature of the plumb line. The determination of the geoid by the astro-gravimetric method also necessitates the surface deflections and the goidal deflections to be

compatible. This compatibility is brought through the application of a correction due to the curvature of the plumb line.

A few researchers such as Helmert(1880), Graaff-Hunter and Bomford(1928), Ledersteger (1955), Arnold(1956), Ndyetabula(1974), Groten(1981) and others have investigated the problem of the curvature of the plumb line. The plumb line curvature effect of the actual gravity field is more important but extremely difficult to determine (Groten, 1981). So far some approaches for the estimation of the curvature effect of the plumb line have been developed: using the gravity field models, using a relation between the curvature effect and orthometric height correction, using density models, and by using Vening Meinesz's and Molodenskij's formulae together, etc. These will be introduced in Chapter 3.

The curvature of the plumb line is mainly due to the topographic irregularity and the density distribution within the earth. In the Alps, the curvature effects of the plumb line up to 12" have been obtained (Kobold and Hunziker, 1962). Without knowledge of the density distribution inside the earth, the accuracy of the plumb line curvature effect obtained by using the first three methods is questionable (Ndyetabula, 1974). Utilizing the first two approaches, a dense gravity net around the computation point is needed (Heiskanen and Moritz, 1967). With the use of Vening

Meinesz's and Molodenskij's formulae, it becomes complicated and time-consuming to compute the geoidal and Molodenskij's deflections separately. Besides, the integrations should be extended over the whole earth.

Using the above mentioned ways, the evaluation of the curvature effect is a difficult task due to the fact that sufficient gravity and height data or the data for the density distribution inside the earth are necessary.

In this study, an alternative approach, developed by Vaníček and Krakiwsky (1982), is used to evaluate the effect of the curvature of the plumb line. The method is based on the combination of Stokes's and Molodenskij's approaches. An analytical form is given of the difference between the geoidal and Molodenskij's deflections. In this thesis, the analytical form is called the Stokes-Molodenskij formula. This formula can compute the plumb line curvature effect more conveniently than Vening Meinesz's and Molodenskij's formulae together. In addition, the distant zones can be neglected without the loss of accuracy, and the density distribution is not needed to determine the plumb line curvature effect.

If the geoidal and the surface deflections are known, the plumb line curvature effect can be straightforwardly determined. In this study, a comparison between the plumb line curvature effect determined from the Stokes-Molodenskij formula and that obtained from the geoidal and the surface

deflections is made at six stations in the province of New Brunswick.

A few definitions and basic philosophical backgrounds are outlined in Chapter 2. In Chapter 3, Stokes's and Molodenskij's approaches for evaluating the deflections of the vertical are given briefly. Some approaches for computing the plumb line curvature effect are also reviewed. The mathematical development of the method combining Stokes's and Molodenskij's approaches to determine the curvature effect is given.

For practical evaluation of the curvature effect of the plumb line by means of the Stokes-Molodenskij formula, there are two different zones needed: innermost and inner. The data used include the point gravity anomalies and heights, and the mean gravity anomalies and mean heights for the 5x5 minutes blocks used. The estimation of the tangent of the terrain inclination is rigorously treated to give a reliable contribution to the plumb line curvature effect. The possibility of neglecting the distant regions beyond the inner zone without affecting accuracy is discussed in Chapter 4.

There are six stations tested, two in mountainous areas and four in flat areas. The results are presented in Chapter 5. For convenience, the curvature effect determined from the Stokes-Molodenskij formula is called the Stokes-Molodenskij curvature effect, and the curvature effect

obtained from the geoidal and the surface deflections is called the astro-gravimetric curvature effect. A comparison between them is also shown in this chapter. The analysis and explanation for the comparison are given. Finally, a few conclusions are drawn and recommendations are given for further studies.

As a guide to the reader, the goal of each chapter is presented below:

1. The goal of Chapter 2 is to review the general concepts for the gravity field of the earth and give an insight into the topic. Three types of the deflections of the vertical used in geodesy and the differences among them were described.
2. The goal of Chapter 3 is to review and relate the different approaches for evaluating the curvature effect of the plumb line. In addition, the mathematical developement of the method based on combining Stokes's and Molodenskij's approaches is also reviewed. The approach can compute the plumb line curvature effect without the knowledge of the density distribution inside the earth and to a high accuracy.
3. The goal of Chapter 4 is to perform a practical evaluation of the Stokes-Molodenskij formula. It is shown that the distant zones whose spherical distances from the computation point exceed 13 can be

neglected without any loss of accuracy. In order to get reliable results, the evaluation of the terrain slope was treated rigorously.

4. The goal of Chapter 5 is to demonstrate the computational results and make comparisons between the Stokes-Molodenskij and the astro-gravimetric curvature effects. The comparisons show that the model based on the Stokes-Molodenskij formula can give a much higher accuracy than the astro-gravimetric model. Besides, the former can be easily applied to evaluate the curvature effect of the plumb line.

A few contributions are made in this work. These are summarized below:

1. First practical testing of the Stokes-Molodenskij formula, developed by Vaníček and Krakiwsky (1982), for the determination of the curvature effect of the plumb line.
2. Development of an algorithm for numerical evaluation of the Stokes-Molodenskij formula.
3. Formulation of an algorithm for terrain slope evaluation.

CHAPTER 2

DEFINITIONS AND GENERAL BACKGROUND

2.1 GRAVITY POTENTIAL, EQUIPOTENTIAL SURFACE, AND PLUMB LINE

A body rotating with the earth is subjected to the gravitational force due to the mass of the earth and the centrifugal force due to the earth's rotation. The sum of the gravitational and the centrifugal forces is called the force of gravity.

The magnitude of the force of gravity is not the same everywhere on the surface of the earth; namely, it is a function of position. The gravity force on the neighborhood of the poles is greater than it is on the equator. In addition, the gravity force undergoes temporal variations resulting from the gravitational force of celestial bodies, crustal deformations, and tectonic deformations (Vaníček and Krakiwsky, 1982).

There is a potential corresponding to the gravity force, called the potential of gravity, W. It is the sum of the gravitational potential, denoted by Wg, and the centrifugal potential, denoted by Wc (Heiskanen and Moritz, 1967):

$$W = Wg + Wc \; . \qquad (2.1)$$

The gradient vector of W,

$$\vec{g} = \nabla W \tag{2.2}$$

is called the gravity field. The magnitude of g is measured in gals (1 gal = 1 $cm \cdot sec^{-2}$ = 1 dyne/g) or in metres per second squared. The sciences of geodesy and geophysics have adopted the more suitable unit --- the milligal (1 mgal = 10^{-3} gal). The direction of the gravity vector is known as the direction of the plumb line, or the vertical.

The term equipotential surface means a surface on which the potential W is constant. The general equation of an equipotential surface is expressed by

$$W(\vec{r}) = const. \tag{2.3}$$

It is a continuous and smooth surface. Although an infinite number of equipotential surfaces can be accredited by different values to the potential, they never intersect one another. The equipotential surfaces define the horizontal direction; thus they are also called level surfaces. The lines of gravity force normal to the earth's equipotential surfaces at every point are called the plumb line (Fig.2.1). Because of the uneven density distribution of the earth, the plumb lines are curved and twisted (Vaníček and Krakiwsky, 1982).

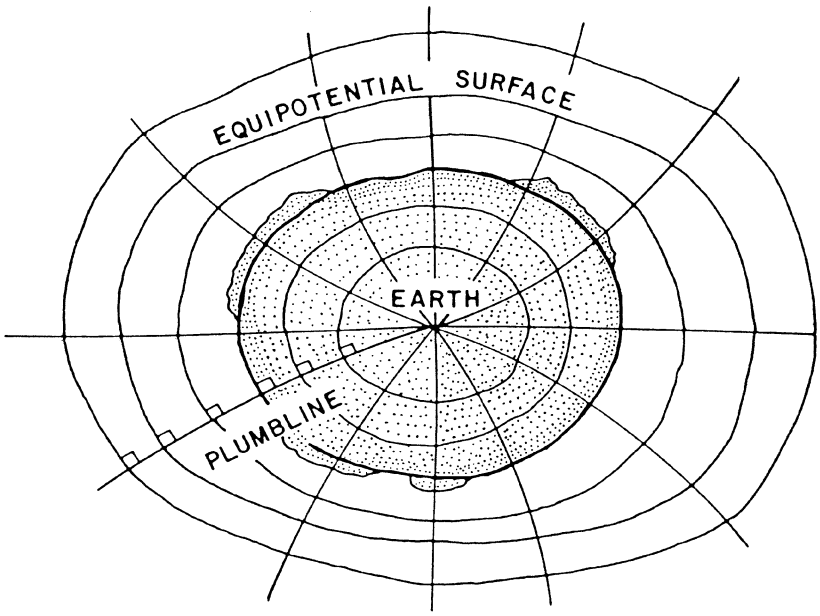

Figure 2.1: Equipotential surfaces and plumb lines (Vaníček and Krakiwsky, 1982).

2.2 REFERENCE ELLIPSOID AND NORMAL GRAVITY FIELD

The Bureau Gravimetrique Internationale in Paris, an institution of the IAG, maitains worldwide gravity data. A few million observations show that the magnitudes of gravity vary locally and regionally. Due to the elevation of stations, the oblateness of the earth, and the uneven mass distribution within the earth, the variations reach more than 5 gals for the magnitude of gravity g (Vaníček and Krakiwsky, 1982).

For geodetic purposes, a reference gravity field is selected such that the average difference between this field and the actual gravity field is as small as possible. An approximate represention of the actual gravity potential may be achieved by an ellipsoid.

A reference ellipsoid is an ellipsoid of revolution which is an equipotential surface of a normal gravity field. It is also called the level ellipsoid. The reference ellipsoid possesses the following characteristics:

1. The mass of the reference ellipsoid is equal to the total mass of the earth, including the mass of the atmosphere.
2. It spins around its minor axis with the same angular velocity as that of the earth.
3. Its center coincides with the gravity center of the earth.

The reference ellipsoid generates a reference gravity field, called normal gravity field. A reference potential, denoted by U, is usually adopted to approximate the actual potential. In analogy to (2.2), the normal gravity vector is given by

$$\vec{\gamma} = \nabla U \ . \tag{2.4}$$

The Geodetic Reference System 1967(GRS67), a geocentric equipotential ellipsoid, adopted at the XIV General Assembly of IUGG in 1967, represents the size, shape, and gravity field of the earth. The primary geometric ellipsoidal parameters are:

equatorial radius(major semi-axis) a = 6378160 metres

flattening of reference ellipsoid f = 1/298.247 .

The corresponding normal gravity γ of level ellipsoid is given by

$$\gamma = 978031.8(1+0.005\ 3024\cdot\sin^2\phi-0.000\ 0059\cdot\sin^2 2\phi) \text{ mgals.} \tag{2.5}$$

It was perceived that GRS67 no longer approximates the actual figure and gravity field of the earth to an adequate accuracy. Therefore, it was replaced by the Geodetic Reference System 1980, also based on the theory of the geocentric equipotential ellipsoid (Moritz, 1980a). The parameters are a= 6378137 metres and f=1/298.257. The international gravity formula(1980) is given by

$$\gamma = 978032.7(1+0.005\ 3024\cdot\sin^2\phi-0.000\ 0058\cdot\sin^2 2\phi)\ \text{mgals}, \quad (2.6)$$

where ϕ is the latitude of station.

2.3 GEOID AND GEOIDAL HEIGHT

The geoid is an equipotential surface of the earth's gravity field which is approximately represented by mean sea level. The geoid is known as the datum for orthometric height system. Besides, the geoid is often referred to as the figure of the earth, because it closely approximates about 72% of the terrestrial globe.

The separation between the geoid and a reference ellipsoid is the geoidal height N (Fig.2.2). At present, there are several possible methods of geoid determination: gravimetric method, astro-geodetic method, astro-gravimetric method, satellite geodynamics, satellite altimetry, direct determination from 3D positions and orthometric heights (Rizos, 1982), etc. It is not within the scope of this thesis to give a description of all the techniques.

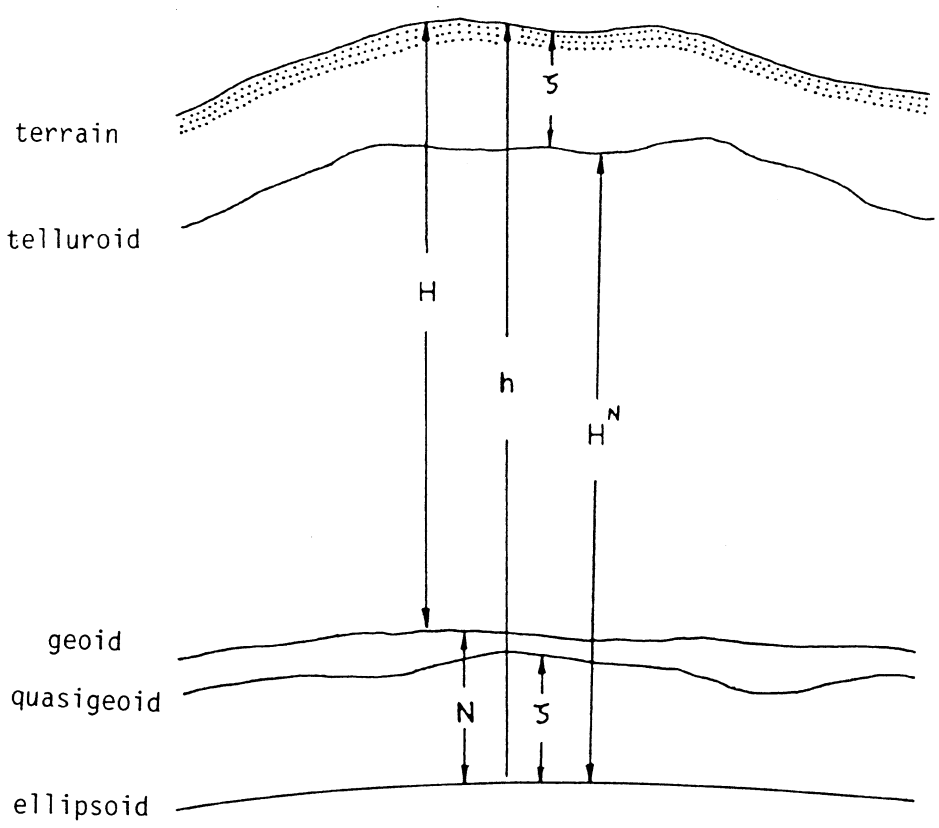

Figure 2.2: Geoid, quasigeoid and telluroid.

2.4 DISTURBING POTENTIAL AND GRAVITY ANOMALY

For the gravity field of the earth, the actual potential W at any point can be expressed by the sum of a normal potential U and a small remainder T:

$$W(\vec{r}) = U(\vec{r}) + T(\vec{r}) \,, \tag{2.7}$$

or

$$T(\vec{r}) = W(\vec{r}) - U(\vec{r}) \,. \tag{2.8}$$

The difference T between the actual potential and the normal potential is called disturbing potential, or anomalous potential. Similarly, the gravity g_p at P is approximated by the corresponding normal gravity γ_Q at point Q on the equipotential surface $U=U_Q$ (Fig.2.3).

The difference in magnitude between them is known as the gravity anomaly at the point P:

$$\Delta g = |\vec{g}_p| - |\vec{\gamma}_Q| \,. \tag{2.9}$$

The vertical gradient of T is given by:

$$\nabla T(\vec{r}_p) = \nabla(W(\vec{r}_p) - U(\vec{r}_p)) = \nabla(W_p - U_p) \,. \tag{2.10}$$

After inserting (2.2) and (2.4) into (2.10), the vertical gradient of the disturbing potential becomes

$$\nabla T = -\frac{\partial T}{\partial n'} = g_p - \gamma_p \,, \tag{2.11}$$

were n' is the ellopsoidal normal (Fig.2.3).

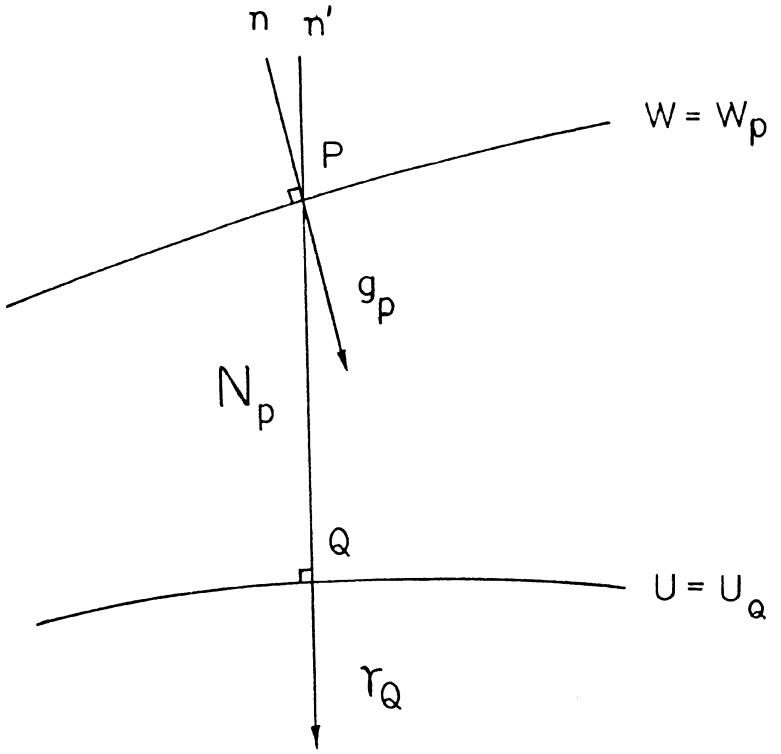

Figure 2.3: Gravity vectors on the actual and the normal potential surfaces.

The normal gravity γ_p at point P may be evaluated by the following linear form (Heiskanen and Moritz, 1967, p.85):

$$\gamma_p = \gamma_a + \frac{\partial \gamma}{\partial n'} \cdot N_p \quad . \tag{2.12}$$

Substituting (2.12) into (2.11) yields

$$-\frac{\partial T}{\partial n'} = g_p - \gamma_a - \frac{\partial \gamma}{\partial n'} \cdot N_p \tag{2.13}$$

or

$$-\frac{\partial T}{\partial n'} = \Delta g - \frac{\partial \gamma}{\partial n'} \cdot N_p \quad . \tag{2.14}$$

Since the relation between the geoidal height and the disturbing potential is given by Bruns as (Ibid., p.85)

$$N = \frac{T}{\gamma} \tag{2.15}$$

and if the directions of geoidal normal n and ellipsoidal normal n' are considered to almost coincide, equation (2.14) becomes

$$-\frac{\partial T}{\partial n} = \Delta g - \frac{\partial \gamma}{\partial n} \cdot \frac{T_p}{\gamma_p} \quad . \tag{2.16}$$

Rearranging (2.16) and disregarding the subscripts, we have

$$\frac{\partial T}{\partial n} - \frac{1}{\gamma} \cdot \frac{\partial \gamma}{\partial n} \cdot T + \Delta g = 0 \quad . \tag{2.17}$$

This expression is known as the fundamental equation of physical geodesy.

2.5 TELLUROID, QUASIGEOID, AND HEIGHT ANOMALY

Two reference surfaces, the reference ellipsoid and the geoid, are used in the conventional approach to the determination of the figure of the earth. Molodenskij proposed a different approach in 1945. In Molodenskij's approach the reference surface is no longer the geoid but the telluroid. There are two different surfaces defined in this approach, telluroid and quasigeoid. The quasigeoid does not have a physical interpretation, except at sea.

The telluroid is originally defined as the locus of points whose normal potential U is equal to the actual potential Wp at the surface of the earth. On the other hand, the telluroid can also be defined as a locus of normal heights H^N measured along the normal plumb line from the reference ellipsoid (Vaníček, 1974).

The separation between the terrain and the telluroid is called height anomaly, denoted by ζ. A locus of height anomalies reckoned along the normal plumb line from the ellipsoid is known as the quasigeoid.

From fig.2.3 , the relationship between the height anomaly ζ and the geoidal height N can be deduced from the following equations:

$$\zeta = h - H^N \qquad (2.18)$$

$$N = h - H \ , \qquad (2.19)$$

where h is ellipsoidal height, and H is orthometric height. It is instructive to compare the height anomaly and geoidal height. Combining equations (2.18) and (2.19) yields

$$N - \zeta = H^N - H \ . \tag{2.20}$$

This difference is fairly small and elevation-dependent. For instance, the difference is about -1.8 m for Mt. Blanc in the Alps (Arnold, 1960). In the open ocean the geoid and quasigeoid coincide, so $N=\zeta$.

2.6 DEFLECTIONS OF THE VERTICAL

The deflection of the vertical is defined as the spatial angle between the normal gravity vector and the actual gravity vector. The deflection of the vertical can be decomposed into two orthogonal components, the north-south (along the astronomical meridian) and the east-west (in the prime vertical) components, denoted by ξ and η . For instance, if the geodetic reference ellipsoid is aligned to the Conventional Terrestial coordinate system(CT), and if astronomic coordinates and geodetic coordinates are denoted by (Φ,Λ) and (ϕ,λ), respectively, then the components of the deflection of the vertical are given by:

$$\begin{aligned} \xi &= \Phi - \phi \\ \eta &= (\Lambda - \lambda)\cdot\cos\phi \ , \end{aligned} \tag{2.21}$$

The origin of the CT system is at the centre of mass of the earth, z-axis points to the Conventional International Origin(CIO), the xz-plane contains the mean Greenwich Observatory, and the y-axis is selected to make the system right-handed.

The deflection obtained can be either absolute or relative according to which kind of reference ellipsoid is adopted. If a non-geocentric ellipsoid is used, it will result in the relative deflection of the vertical. The deflection, however, is absolute when the adopted reference ellipsoid is geocentric.

It should be mentioned here that there are three species of deflection used in geodesy. These are:

1. The surface deflection of the vertical θ', defined as the angle at the surface of the earth between the directions of the plumb line and the normal (through point P) to the reference ellipsoid (Fig.2.4). The deflection components are denoted by ξ' and η'. The surface deflection can be obtained from astronomic observations. The actual or normal gravity is not required.
2. The geoidal deflection of the vertical θ is defined as the angle (on the geoid) between the directions of the plumb line and the ellipsoidal normal (through point Po), see Fig.2.5. The components of the deflection are denoted by ξ and η.

3. Molodenskij's deflection of the vertical $\tilde{\theta}$ is defined by Molodenskij as the angle between the directions of the plumb line (at point P) and the normal (through point P) to the telluroid (Fig.2.5). The deflection components are denoted by $\tilde{\xi}$ and $\tilde{\eta}$.

Clearly, due to the curved and twisted plumb line the surface and geoidal deflections for the same point (with respect to the same reference ellipsoid) are different. Ordinarily, the differences between them are expected to be more significant in mountainous areas than in the flat-terrain regions. In the Alps, the differences of up to 12" have been obtained by Kobold and Hunziker(1962).

The surface deflections are also different from Molodenskij's deflections. The deviation coming from the curvature of the normal plumb line between the ellipsoid and the telluroid is a function of the latitude and height of the computation station. Greater differences occur at the higher elevations.

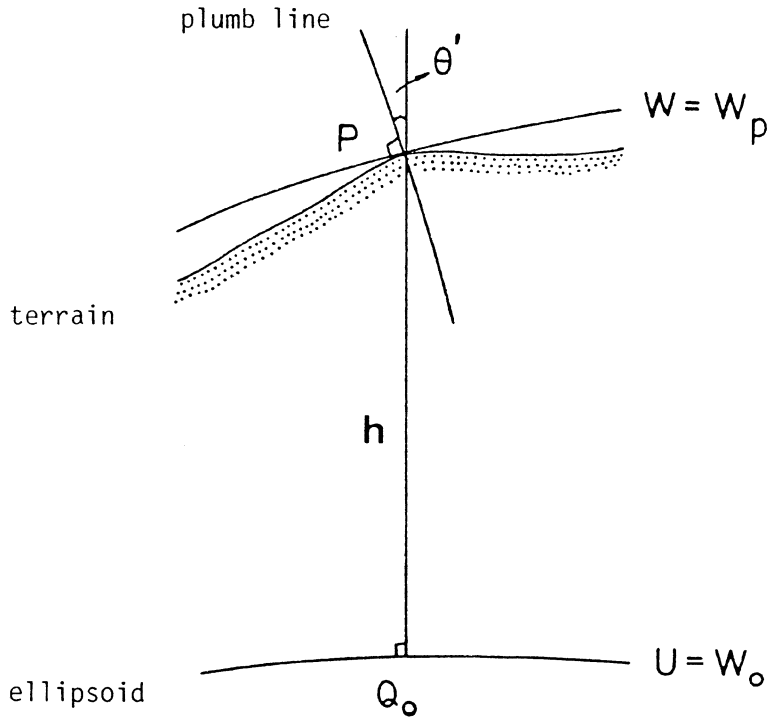

Figure 2.4: Surface deflection (or astro-geodetic deflection).

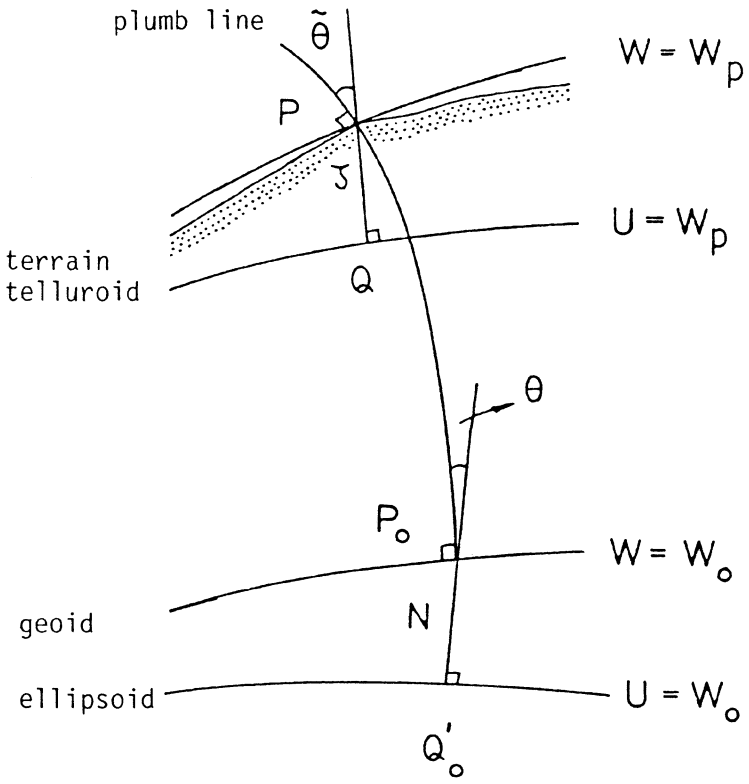

Figure 2.5: Molodenskij's deflection and geoidal deflection.

CHAPTER 3

MATHEMATICAL DEVELOPMENT FOR THE CURVATURE EFFECT OF THE PLUMB LINE

3.1 GEOIDAL DEFLECTION OF THE VERTICAL

The geoidal deflection mentioned in the preceding chapter is the angle between the actual gravity vector on the geoid and the normal gravity vector on the reference ellipsoid. The determination of the geoidal deflections is one of the tasks in geodesy, since it is usually required for geodetic purposes. In Stokes's approach to the geodetic boundary-value problem the geoid serves as a physical reference surface. It must be assumed that there are no masses outside the geoid, otherwise the theorem of Stokes is not valid to determine the deflection of the vertical as well as the geoid by means of gravity. In fact, there are masses above the geoid, so they must be either completely removed or moved inside the geoid. For this reason, some assumptions and hypotheses concerning the density of mass above the geoid must be made. The gravity measured on the surface of the earth, therefore, has to be reduced downward to the geoid.

If gravity has already been reduced to the geoid appropriately, then the gravity anomaly Δg on the geoid can

be obtained. In geodesy, the free-air gravity anomalies are used to determine the geoidal height and the geoidal deflection of the vertical. The derivation of the formulae for determining the deflections has been described in a few texts(e.g. Heiskanen and Vening Meinesz, 1958; Heiskanen and Moritz, 1967; Vanicek and Krakiwsky, 1982). It will not be discussed here. The formulae, referred to as the Vening Meinesz formulae, are:

$$\xi = \frac{1}{4\pi\gamma_m}\cdot\iint_{\nu}\Delta g\cdot\frac{dS(\psi)}{d\psi}\cdot\cos\alpha\cdot d\nu$$
$$\eta = \frac{1}{4\pi\gamma_m}\cdot\iint_{\nu}\Delta g\cdot\frac{dS(\psi)}{d\psi}\cdot\sin\alpha\cdot d\nu \quad , \tag{3.1}$$

where γ_m is the mean normal gravity on the ellipsoid,

Δg is the free-air gravity anomaly,

ψ is the spherical distance between the computation point P and the dummy point P' (Fig.3.1),

α is the azimuth of the line PP', and

$d\nu$ is a solid angle element (ν is the spherical surface of the earth).

$dS(\psi)/d\psi$, known as the Vening Meinesz function, is given by (Heiskanen and Moritz, 1967, p.114):

$$\frac{dS(\psi)}{d\psi} = \frac{-\cos(\psi/2)}{2\sin^2(\psi/2)} + 8\sin(\psi) - 6\cos(\psi/2) - 3\cdot\frac{1-\sin(\psi/2)}{\sin(\psi)}$$
$$+ 3\sin(\psi)\cdot\ln\left(\sin(\psi/2)+\sin^2(\psi/2)\right). \tag{3.2}$$

and Δg is written as:

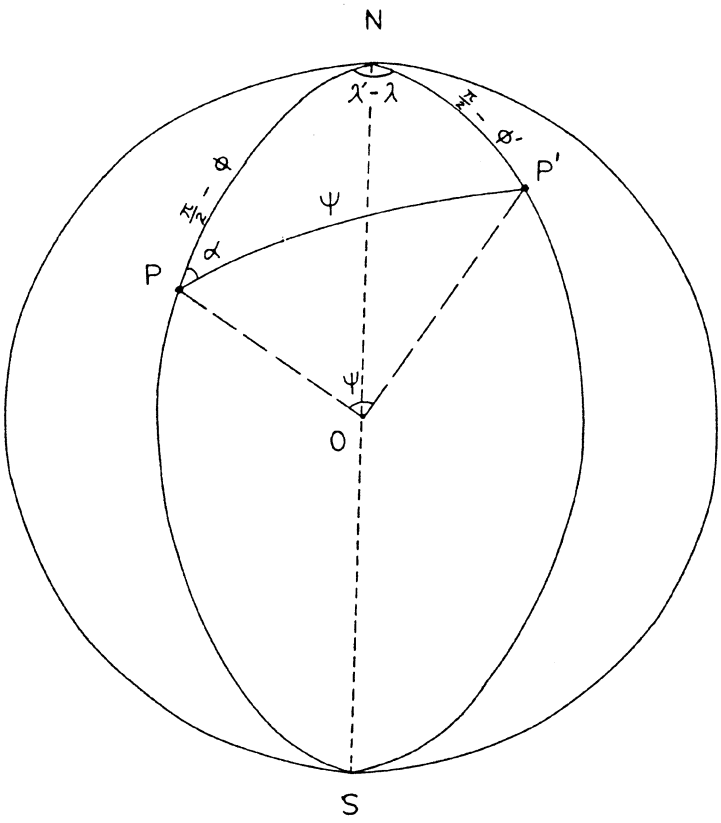

Figure 3.1: Geometry of a sphere and its sections.

$$\Delta g = g + 0.3086 \cdot H - \gamma_o \ , \qquad (3.3)$$

where g is the observed gravity in mgals on the surface of the earth, γ_o is the normal gravity in mgals on the ellipsoid, H is the orthometric height of the observation point in metres, and the factor 0.3086 is in mgal/m.

3.2 MOLODENSKIJ'S DEFLECTION OF THE VERTICAL

In 1945, Molodenskij proposed a different approach to formulate the geodetic boundary-value problem for the earth's surface without a hypothesis. The reference surface is not the geoid but the telluroid. In Molodenskij's approach the actual potential W on the earth's surface is approximated by a normal potential U on the telluroid, and the disturbing potential T is taken for the point on the earth's surface. Accordingly, in this approach, the gravity anomaly is a boundary value on the surface of the earth. The gravity anomaly on the earth's surface, denoted by $\Delta\tilde{g}$, is called the surface gravity anomaly here. It is the difference between the actual gravity on the earth's surface and the normal gravity on the telluroid, given by:

$$\Delta\tilde{g} = g - (\gamma_o - 0.3086 \cdot H^N) \ . \qquad (3.4)$$

The deflection of the vertical in Molodenskij's theory, mentioned in the preceding chapter, is an angle between the actual gravity vector on the earth's surface and

the normal gravity vector on the telluroid. Molodenskij's formulae for the deflections, based on the first approximation for the surface layer density, are the following (Molodenskij et al, 1962; Heiskanen and Moritz, 1967; Vaníček and Krakiwsky, 1982):

$$\tilde{\xi} = \frac{1}{4\pi\gamma}\iint_{\nu}\left(\Delta\tilde{g} + \Delta G\right)\cdot\frac{dS(\psi)}{d\psi}\cdot\cos\alpha\cdot d\nu - \frac{\Delta\tilde{g}}{\gamma}\cdot\tan\beta_1$$
$$\tilde{\eta} = \frac{1}{4\pi\gamma}\iint_{\nu}\left(\Delta\tilde{g} + \Delta G\right)\cdot\frac{dS(\psi)}{d\psi}\cdot\sin\alpha\cdot d\nu - \frac{\Delta\tilde{g}}{\gamma}\cdot\tan\beta_2, \qquad (3.5)$$

where

$$\Delta G = \frac{R^2}{2\pi}\iint_{\nu}\frac{H^N - H_P^N}{s^3}\left(\Delta\tilde{g} + \frac{3\gamma}{2R}\cdot\zeta\right)\cdot d\nu \qquad (3.6)$$

and

$$\zeta = \frac{R}{4\pi\gamma}\iint_{\nu}\left(\Delta\tilde{g} + \Delta G\right)\cdot S(\psi)\cdot d\nu\ , \qquad (3.7)$$

where γ is the normal gravity on the telluroid,

R is the mean radius of the earth,

β_1, β_2 are the terrain inclinations in the north-south and the east-west directions, respectively,

H_P^N, H^N are the normal heights of the computation point P and the dummy point P', respectively(Fig.3.2),

s is the distance between P and P', and

$S(\psi)$ is Stokes's function.

R, s, and $S(\psi)$ are given by:

$$R = \sqrt[3]{a^2 b}\ , \text{ or } \quad R = a\cdot(1 - f)^{1/3}, \qquad (3.8)$$

$$s = 2R\sin(\Psi/2) \ , \tag{3.9}$$

$$S(\Psi) = \frac{1}{\sin(\Psi/2)} + 1 - 5\cos(\Psi) - 6\sin(\Psi/2) - 3\cos(\Psi)\cdot \ln\left(\sin(\Psi/2) + \sin^2(\Psi/2) \right) \ . \tag{3.10}$$

According to the different theories and the different definitions, Molodenskij's deflections are indeed different from the surface and the geoidal deflections. The difference between Molodenskij's deflection and the surface deflection arising from the curvature of the normal plumb line is only about 0.85 arcseconds for Mt. Blanc in the Alps. However, the difference between the geoidal deflection and the surface deflection was up to 12 arcseconds at the same place (Kobold and Hunziker, 1962). It is obvious that Molodenskij's deflection is always much closer to the surface deflection than to the geoidal deflection in mountainous area.

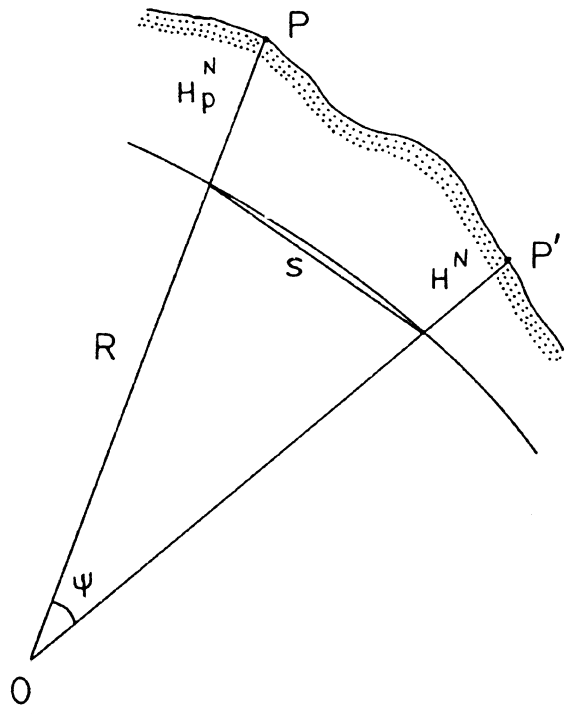

Figure 3.2: Spherical approximation.

3.3 SOME TECHNIQUES FOR COMPUTING THE CURVATURE EFFECT OF THE PLUMB LINE

The plumb line, the so-called line of gravity force, is bent and twisted. Some of the geodetic measurements on the physical surface of the earth, e.g. triangulation and levelling, make use of the plumb line. For some geodetic missions, the influence of the curvature of the plumb line should be taken into account when the reduction of geodetic or astronomic observations to the geoid or to the ellipsoid is needed. No matter how the plumb lines bend and twist within the earth, the curvature effect of the plumb line between the earth's surface and the geoid is usually considered in the field of geodesy. That is to say, that the deviation between the gravity vector on the earth's surface and the gravity vector on the geoid is investigated. It is also convenient for geodetic purposes to decompose the curvature effect, denoted by $\Delta\theta$, into the north-south component $\Delta\xi$ and the east-west component $\Delta\eta$ as the same way as the deflection of the vertical is decomposed.

There are a few ways of determining the curvature effect of the plumb line: by using the gravity field models, by using a relation between the curvature effect and orthometric height correction, by using density models, by using Vening Meinesz's and Molodenskij's formulae together, etc.

3.3.1 Using the gravity field models

Taking the origin at the computational point, we set up a rectangular coordinate system xyz with z-axis along the vertical and the x- and y-axes on the horizontal plane pointing northwards and eastwards, respectively. Such a system is called the Astronomical system(LA).

The two orthogonal components of the plumb line curvature effect are given by (Heiskanen and Moritz, 1967):

$$\Delta\xi = -\int_o^H \frac{1}{g}\cdot\frac{\partial g}{\partial x}\,dh$$

$$\Delta\eta = -\int_o^H \frac{1}{g}\cdot\frac{\partial g}{\partial y}\,dh, \qquad (3.11)$$

where H is the orthometric height of the computation point. In order to evaluate the above integrals, a knowledge of the gravity and its horizontal gradients at every point along the plumb line is necessary. Because the density distribution and the gravity variations inside the earth are not well-known, it is difficult to evaluate the curvature effect of the plumb line from these formulae.

If the actual gravity g is replaced by the normal gravity γ in the equation (3.11), the curvature effect of the normal plumb line will be obtained. Using (2.5), we obtain the curvature effect of the normal plumb line:

$$\Delta\xi^{N} = -\,0.17''\cdot\sin 2\Phi\cdot H$$
$$\Delta\eta^{N} = \quad 0\ , \tag{3.12}$$

where H is the orthometric height in kilometres. Since the normal gravity field is independent of longitude, the east-west component is zero.

3.3.2 Using the relation between curvature effect and orthometric correction

This approach is developed on the basis of a relation between the actual plumb line curvature effect (From now on we shall leave out the word "actual".) and the orthometric height correction. The curvature effect of the plumb line is given by the following formulae (Heiskanen and Moritz, 1967):

$$\Delta\xi = -\frac{H}{\bar{g}}\cdot\frac{\partial\bar{g}}{\partial x} + \frac{g-\bar{g}}{\bar{g}}\cdot\frac{\partial H}{\partial x}$$
$$\Delta\eta = -\frac{H}{\bar{g}}\cdot\frac{\partial\bar{g}}{\partial y} + \frac{g-\bar{g}}{\bar{g}}\cdot\frac{\partial H}{\partial y}, \tag{3.13}$$

where $\bar{g}$ is the mean gravity along the plumb line. In order to get reliable results, a dense gravity net around the computation point is necessary to determine the horizontal gradients of mean gravity $\partial\bar{g}/\partial x$ and $\partial\bar{g}/\partial y$, and the determination of mean gravity g along the plumb line must be accomplished carefully. Even though horizontal gradients

of gravity are less sensitive to small density variations than vertical gravity gradient, they are difficult to evaluate precisely (Groten, 1981).

Alternatively, (3.13) may be written as:

$$\Delta\xi\cdot\cos\alpha + \Delta\eta\cdot\sin\alpha = -\frac{H}{\bar{g}}\cdot\frac{\partial\bar{g}}{\partial s} + \frac{g-\bar{g}}{\bar{g}}\cdot\frac{\partial H}{\partial s}\,, \qquad (3.14)$$

where α is the azimuth of section AB going through the computation point P (Fig.3.3).

An alternative model to compute the plumb line curvature effect and the Poincaré-Prey reduction constant by means of the least-squares adjustment is (Ndyetabula, 1974):

$$F = \Delta\xi\cdot\cos\alpha + \Delta\eta\cdot\sin\alpha + \frac{h}{2S}\cdot\left(g - K\cdot h\right)^{-1}$$

$$\cdot\left(g_B - g_A - 4\cdot K\cdot\left(H_B - H_A\right) + \delta\right), \qquad (3.15)$$

where

$$\delta = (-1)^m\cdot\left(\frac{1}{2}\cdot\frac{\partial\gamma}{\partial h} - K\right)\cdot\frac{\left(H_i - h\right)^2}{h} \qquad (3.16)$$

and

$$m = \begin{cases} 0 & \text{when } H_B > H_A \\ 1 & \text{when } H_B < H_A \end{cases} \quad ; \quad H_i = \begin{cases} H_A & \text{if } H_B > H_A \\ h & \text{if } H_B = H_A \\ H_B & \text{if } H_B < H_A \end{cases},$$

where g and h, g_A and H_A, and g_B and H_B are the gravity values and the heights at the computation point, at station A, and at station B, respectively (Fig.3.3). For the derivation of the above formula see Ndyetabula (1974,

pp.49-63). The Poincaré-Prey reduction constant, denoted by K, is given by (Heiskanen and Moritz, 1967):

$$K = \frac{1}{2} \cdot \left(\frac{\partial \gamma}{\partial h} + 4\pi G \rho \right) , \qquad (3.17)$$

where $\partial\gamma/\partial h$ is the free-air vertical gradient of gravity,

G is the gravitational constant, and

ρ is the density of the earth's crust.

If the normal density ρ of 2.67 g/cm^3 is adopted, the Poincaré-Prey reduction constant K is -0.0424 mgal/m. The general form of mean gravity $\bar{g}$ along the plumb line is expressed as:

$$\bar{g} = g - K \cdot H . \qquad (3.18)$$

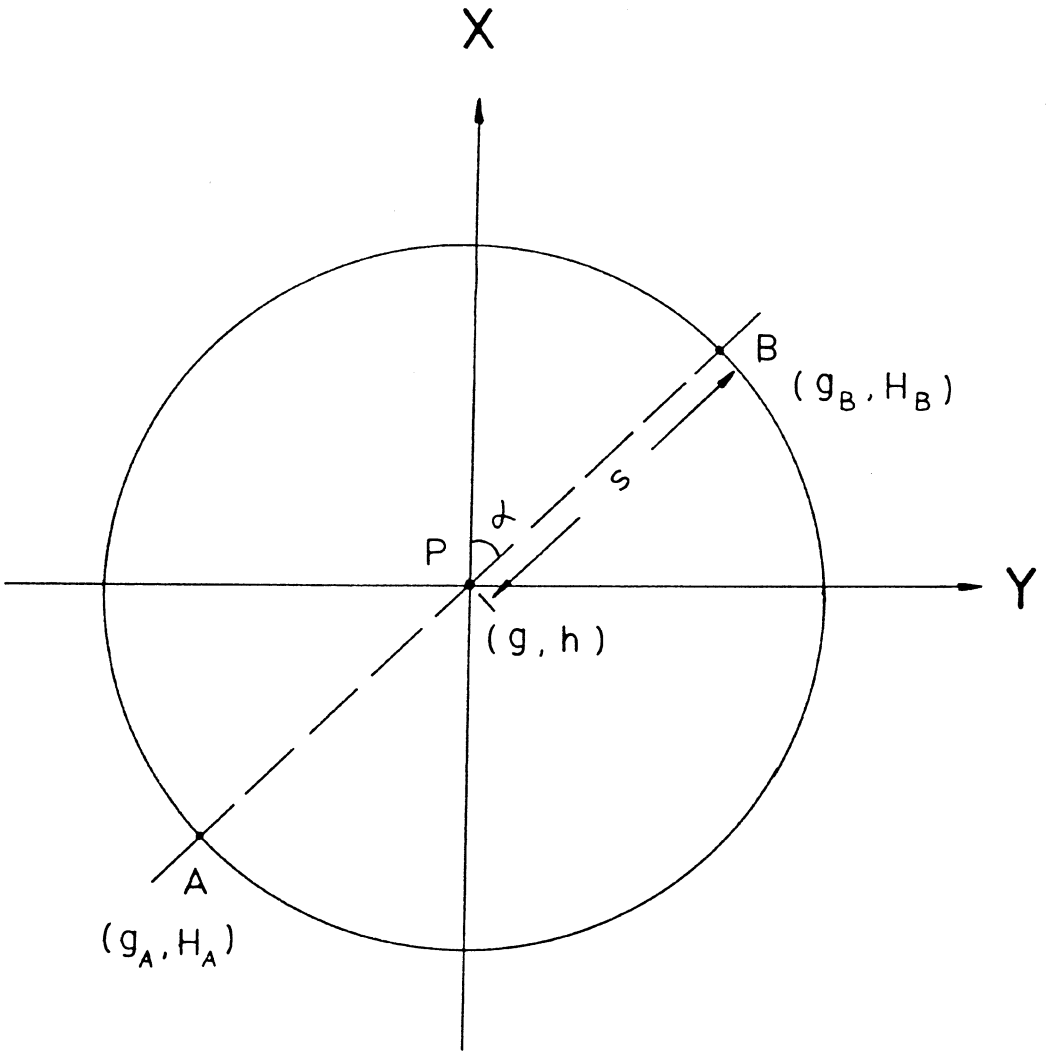

Figure 3.3: Consideration of the plumb line curvature effect for section AB.

3.3.3 Using density models

The point P on the earth's surface and the corresponding point Po on the geoid are subjected to different gravity forces. The direction of the vertical changes from the earth's surface to the geoid due to the irregular mass distribution inside the earth's crust. If the density distribution is known, the deviation between these two directions of the vertical can be determined by Newton's law of gravitation.

The general idea of evaluating the curvature effect of the plumb line using the model will be outlined in this subsection. First, taking a local astronomical coordinate system (Fig.3.4), we define P to be the computation point on the earth's surface, Po to be the corresponding point on the geoid, and Q to be the attracting point. In the figure, the origin O of the system is located on the geoid.

Let us now consider a mass element dm at point Q, and dm is equal to $\rho \cdot dv$, where dv is the volume of the element and ρ is the density of the element. According to Newton's law of gravitation, the resulting force $\vec{dF}$ at P is given by:

$$\vec{dF} = \frac{G \cdot dm}{\ell^3} \cdot \vec{\ell} = \frac{G \cdot \rho \cdot dv}{\ell^3} \cdot \vec{\ell} \,. \qquad (3.19)$$

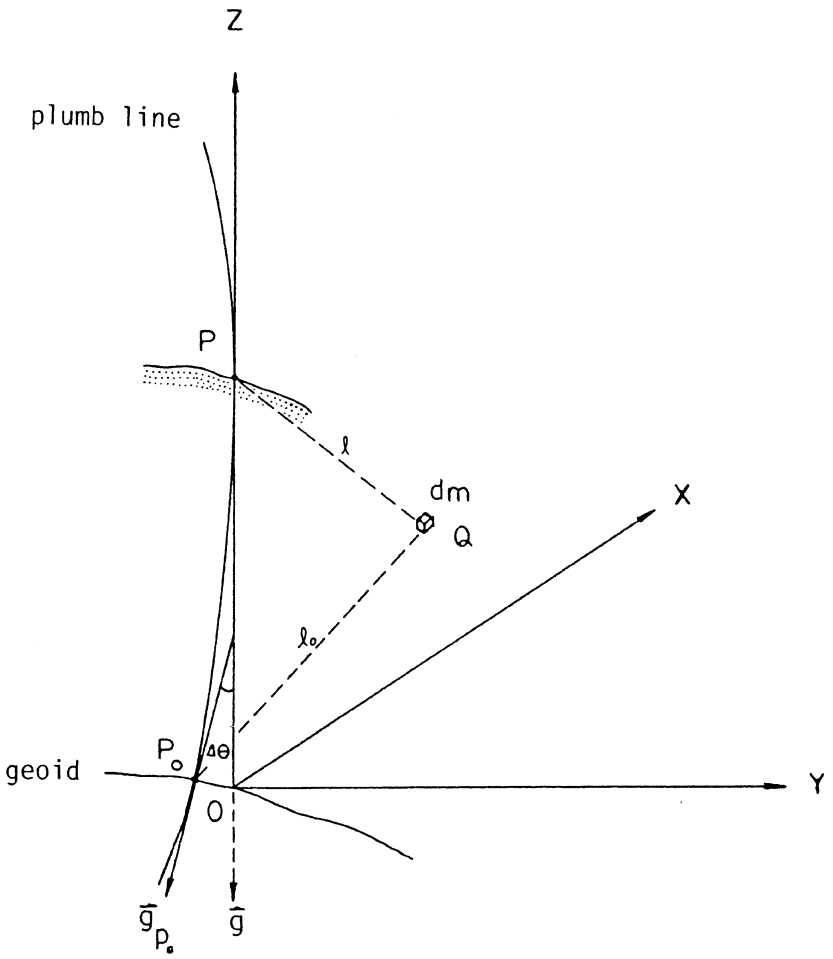

Figure 3.4: A local astronomical coordinate system.

The three components of the force $\vec{dF}$ along the x, y, and z axes respectively are:

$$\vec{dFx} = \frac{G\cdot\rho\cdot dv}{\ell^2}\cos(\vec{\ell}\ ,\ \vec{i}\ )$$

$$\vec{dFy} = \frac{G\cdot\rho\cdot dv}{\ell^2}\cos(\vec{\ell}\ ,\ \vec{j}\ ) \qquad (3.20)$$

$$\vec{dFz} = \frac{G\cdot\rho\cdot dv}{\ell^2}\cos(\vec{\ell}\ ,\ \vec{k}\ ),$$

where $\vec{i}$, $\vec{j}$, and $\vec{k}$ are unit vectors along the x, y, and z axes, respectively. In the coordinate system, the volume of the element dv is equal to dxdydz. Then, the components of the total force $\vec{F}$ are:

$$Fx = G\iiint_V \frac{\rho\cdot\cos(\vec{\ell}\ ,\vec{i}\ )}{\ell^2}\cdot dxdydz$$

$$Fy = G\iiint_V \frac{\rho\cdot\cos(\vec{\ell}\ ,\vec{j}\ )}{\ell^2}\cdot dxdydz \qquad (3.21)$$

$$Fz = G\iiint_V \frac{\rho\cdot\cos(\vec{\ell}\ ,\vec{k}\ )}{\ell^2}\cdot dxdydz\ ,$$

where V is the volume of the earth. Similarly, the three components of total $\vec{F}_o$ at point Po are:

$$Fx_o = G\iiint_V \frac{\rho\cdot\cos(\vec{\ell}_o\ ,\vec{i}\ )}{\ell_o^2}\cdot dxdydz$$

$$Fy_o = G\iiint_V \frac{\rho\cdot\cos(\vec{\ell}_o\ ,\vec{j}\ )}{\ell_o^2}\cdot dxdydz \qquad (3.22)$$

$$Fz_o = G\iiint_V \frac{\rho\cdot\cos(\vec{\ell}_o\ ,\vec{k}\ )}{\ell_o^2}\cdot dxdydz\ .$$

In the coordinate system the z-axis coincides with the gravity vector on the earth's surface, so that the x and y components of force $\vec{F}$ are zero and Fz is equal to -g at the surface of the earth. The curvature effect of the plumb line, therefore, can be obtained from (Fig.3.5):

$$\begin{aligned} \Delta\xi &\doteq \arctan(- Fx_o / Fz_o) \\ \Delta\eta &\doteq \arctan(- Fy_o / Fz_o). \end{aligned} \tag{3.23}$$

In equation (3.22), the evaluations of Fx_o, Fy_o, and Fz_o can be easily done using a circular cylinder method. The volume of the element dV is here equal to rdAdrdz (Fig.3.6), where A is the azimuth of the element. Substituting dv=rdAdrdz into (3.20), the components of $\vec{F}_o$ are given by:

$$\begin{aligned} Fx_o &= G \iiint_V \frac{\rho \cdot \cos(\vec{\ell}_o, \vec{i})}{\ell_o^2} \cdot rdAdrdz \\ Fy_o &= G \iiint_V \frac{\rho \cdot \cos(\vec{\ell}_o, \vec{j})}{\ell_o^2} \cdot rdAdrdz \\ Fz_o &= G \iiint_V \frac{\rho \cdot \cos(\vec{\ell}_o, \vec{k})}{\ell_o^2} \cdot rdAdrdz \ . \end{aligned} \tag{3.24}$$

Integrating (3.24), the x and y components of F are obtained from (Heiskanen and Vening Meinesz, 1958, p.253; Zakatov, 1962, p.193):

$$\begin{aligned} Fx_o &\doteq G \sum_{j=1}^{u} \rho_j \cdot \bar{H}_j (\sin A_2 - \sin A_1) \cdot \ln(r_2/r_1) \\ Fy_o &\doteq G \sum_{j=1}^{u} \rho_j \cdot \bar{H}_j (\cos A_1 - \cos A_2) \cdot \ln(r_2/r_1) \ , \end{aligned} \tag{3.25}$$

where A_1 and A_2, r_1 and r_2 are the boundaries of the compartment,

u is the number of the compartments,

ρ_j is the density of the j-th compartment, and

$\bar{H}_j$ is the mean height above the geoid of the compartment.

The component Fz_o can be approximated by -g at the computation point P:

$$Fz_o = -g \,. \tag{3.26}$$

Unless the density distribution around the point of computation is well known, to calculate the curvature effect of the plumb line, assumptions concerning the density must be made and the heights around the computation point are required. If the assumption that the density is constant is made, only the terrain effect on the plumb line is taken into account without considering the effect of the density distribution. In this approach the uncertainties in estimating the density distribution inside the earth are the predominant error sources. If the distribution of density is not well known, the errors may be very large (Zakatov, 1962).

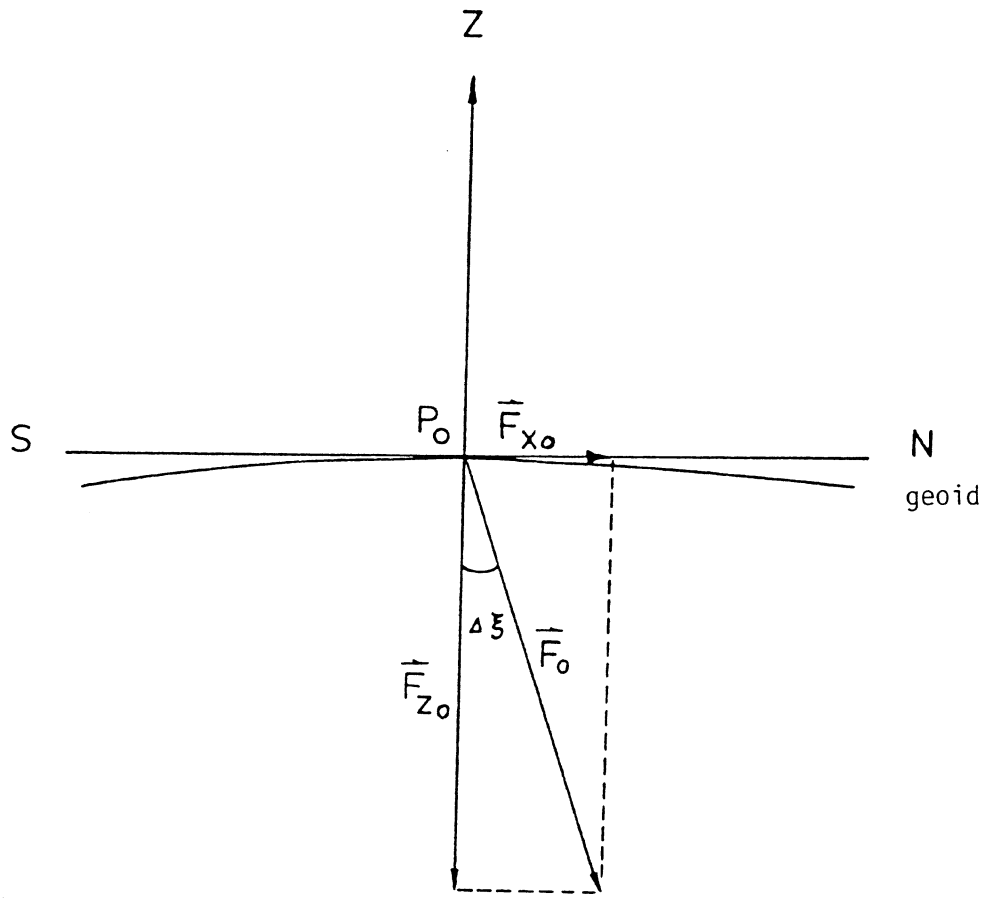

Figure 3.5: The north-south component of the plumb line cruvature effect.

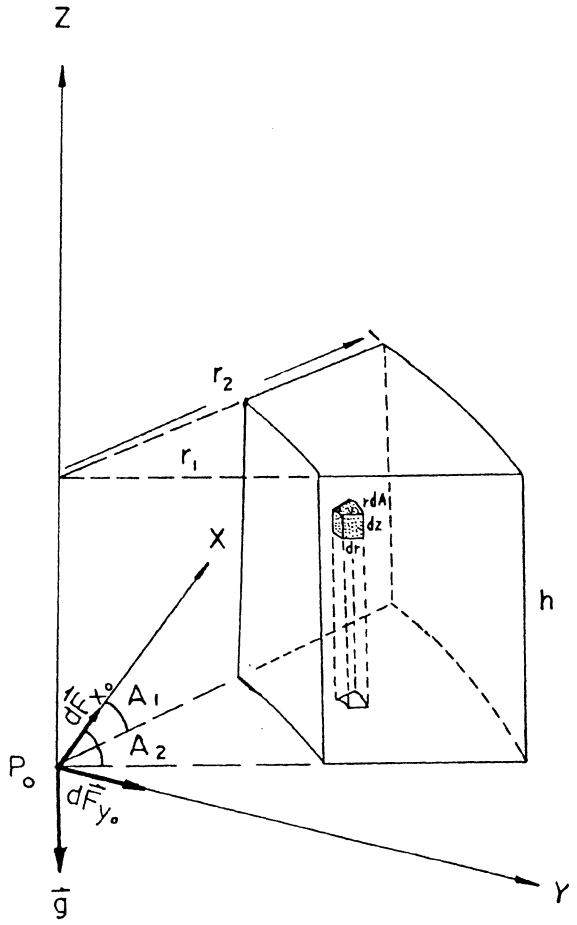

Figure 3.6: Attraction of one compartment.

3.4 STOKES-MOLODENSKIJ METHOD FOR COMPUTING THE CURVATURE EFFECT

The methods of determing the curvature effect of the plumb line outlined in the preceding sections can be regarded as direct ways to compute the deviation between the actual gravity vector on the earth's surface and the actual gravity vector on the geoid. In this section, the possible way of utilizing the geoidal deflection and Molodenskij's deflection to estimate the plumb line curvature effect will be discussed.

If the astronomical coordinates of point P on the earth's surface are denoted by (Φ,Λ) and if they have been corrected for the curvature effect of the actual plumb line, then we get reduced astronomical coordinates (Φ^*,Λ^*) on the geoid (Groten, 1981):

$$\begin{aligned} \Phi^* &= \Phi + \Delta\xi \\ \Lambda^* &= \Lambda + \Delta\eta \ /\cos\Phi . \end{aligned} \tag{3.27}$$

Rearranging (3.27) yields

$$\begin{aligned} \Delta\xi &= \Phi^* - \Phi \\ \Delta\eta &= (\Lambda^* - \Lambda)\cdot\cos\Phi . \end{aligned} \tag{3.28}$$

In Fig.3.7, we use the following notations:

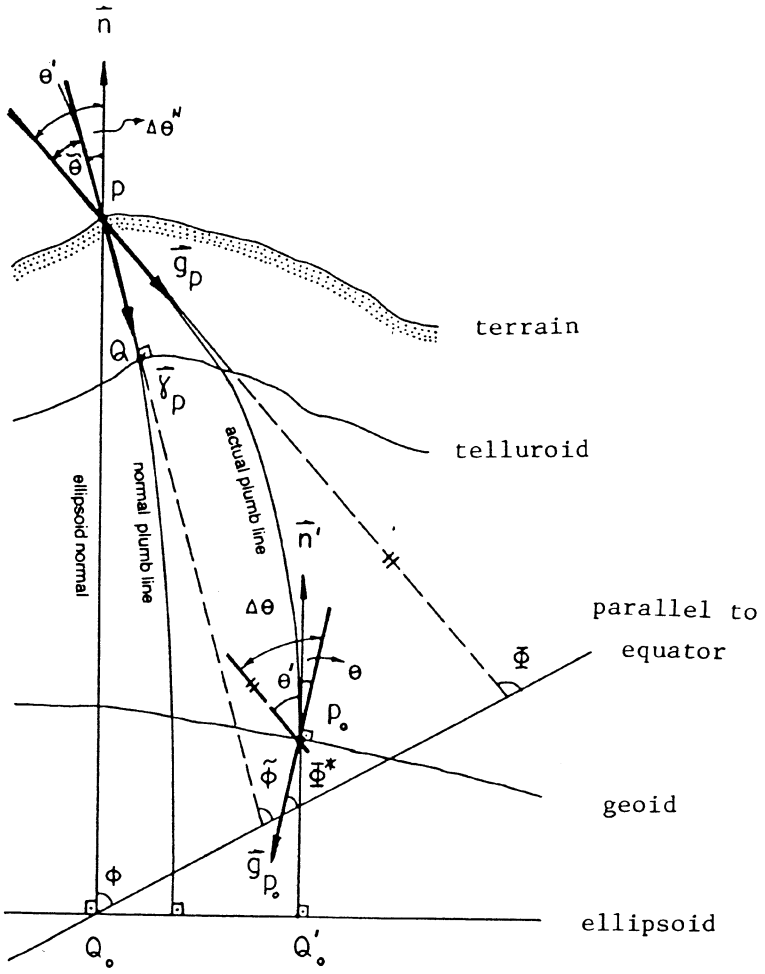

Figure 3.7: Normal and actual plumb line curvature effects.

1. n is the surface normal to the ellipsoid; n' is the geoidal normal to the ellipsoid. For determining the surface deflections, we may neglect the deviation between n and n' (Heiskanen and Moritz, 1967).
2. (Φ, Λ) are the astronomical coordinates at P.
3. (ϕ, λ) are the geodetic coordinates in Helmert's projection system.
4. g_p is gravity at P; g_{p_o} is gravity on the geoid located on the actual plumb line of P_o.
5. γ_p is normal gravity at P.
6. $\Delta\theta^N$ is the deviation between γ_p and n due to the curvature effect of the normal plumb line.
7. $\Delta\theta$ is the deviation between g_p and g_{p_o} due to the curved and twisted plumb line.
8. The rest of the symbols in Fig.3.7 have the same meaning as before.

The equations (3.28) can be rewritten as:

$$\begin{aligned} \Delta\xi &= (\overset{*}{\Phi} - \phi) - (\Phi - \phi) \\ \Delta\eta &= (\overset{*}{\Lambda} - \lambda)\cdot\cos\phi - (\Lambda - \lambda)\cdot\cos\phi . \end{aligned} \tag{3.29}$$

Assuming that three kinds of the deflections are referred to the same ellipsoid (aligned to the CT system), equation (3.29) becomes

$$\begin{aligned} \Delta\xi &= \xi - \xi' \\ \Delta\eta &= \eta - \eta' , \end{aligned} \tag{3.30}$$

or

$$\Delta\theta = \theta - \theta' , \tag{3.31}$$

where θ and θ' are the geoidal deflection and the surface deflection, respectively. If the geoidal and the surface deflections are known, the curvature effect of the plumb line can be straightforwardly obtained by using equations (3.30).

A relation between the surface deflection and Molodenskij's deflection can be obtained from Fig.3.7:

$$\Delta\theta^{N} = \tilde{\theta} - \theta' , \tag{3.32}$$

where $\tilde{\theta}$ is Molodenskij's deflection of the vertical. From equation (3.32), apparently, the difference between these two deflections is caused by the effect of the curvature of the normal plumb line. The east-west component of the curvature effect is equal to zero. Equation (3.32) can be written as:

$$\theta' = \tilde{\theta} - \Delta\theta^{N} . \tag{3.33}$$

Substituting (3.33) into (3.31), we have

$$\Delta\theta = \theta - \tilde{\theta} + \Delta\theta^{N} . \tag{3.34}$$

In order to describe easily the relationship among the three deflections, the situation is summarized in Fig.3.8 .

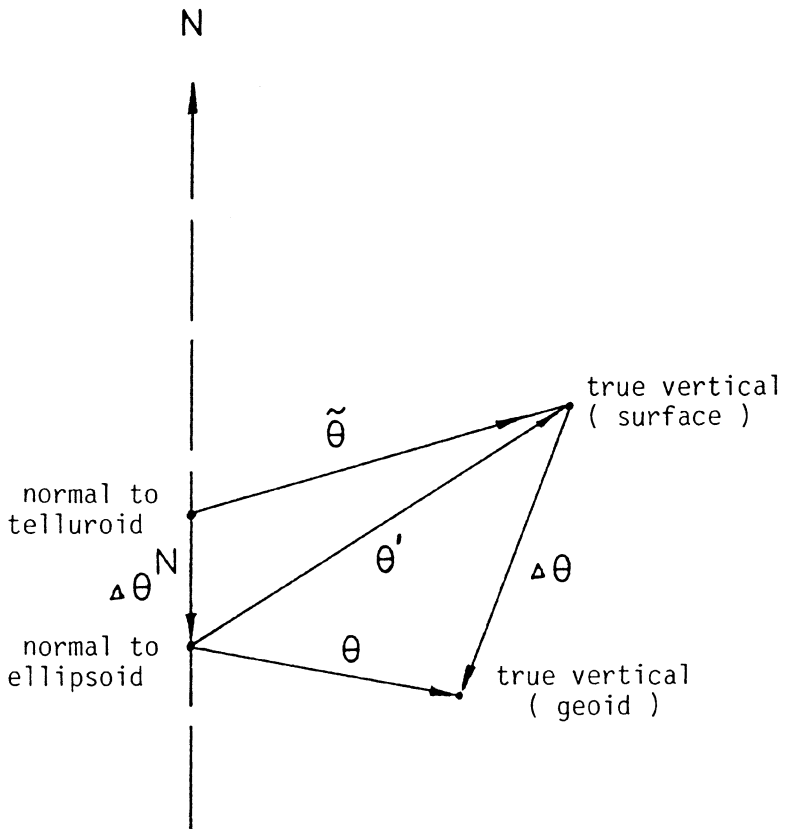

Figure 3.8: Relationship between deflections and curvature effects (Vaníček and Krakiwsky, 1982).

Obviously, if the geoidal deflection and Molodenskij's deflection are available, the curvature effect of the plumb line can be obtained by equations (3.34). These deflections are obtained from Vening Meinesz's formula and Molodenskij's formula. Due to the law of error propagation, the errors of the geoidal deflection and of Molodenskij's deflection will contribute to the errors of the plumb line curvature effect at the computation point. In addition, it is clearly uneconomical to compute the geoidal deflection and Molodenskij's deflection separately. The procedures for the calculation of the geoidal deflection and Molodenskij's deflection are basically the same. It is instructive to compare them.

Referring to equations (3.1) and (3.5), the difference between them is:

$$\theta - \tilde{\theta} = \begin{Bmatrix} \xi \\ \eta \end{Bmatrix} - \begin{Bmatrix} \tilde{\xi} \\ \tilde{\eta} \end{Bmatrix} = \frac{1}{4\pi\gamma_m} \iint_{\nu} (\Delta g - \Delta\tilde{g} - \Delta G) \cdot \begin{Bmatrix} \cos\alpha \\ \sin\alpha \end{Bmatrix} \times \frac{dS(\psi)}{d\psi} \cdot d\nu + \frac{\Delta\tilde{g}}{\gamma_m} \cdot \begin{Bmatrix} \tan\beta_1 \\ \tan\beta_2 \end{Bmatrix} . \qquad (3.35)$$

From (3.3) and (3.4), the difference between the free-air gravity anomaly on the geoid and the gravity anomaly on the earth's surface is obtained from:

$$\Delta g - \Delta\tilde{g} = 0.3086 \cdot (H - H^N) , \qquad (3.36)$$

where H^N can be replaced by $H \cdot \bar{g}/\bar{\gamma}$, and $\bar{\gamma}$ is the mean normal gravity along the normal plumb line, given by (Heiskanen and Moritz, 1967):

$$\bar{\gamma} = \gamma_o - 0.1543 \cdot H^N , \tag{3.37}$$

where the factor 0.1543 is in mgal/m. Substituting the relation $H^N = H \cdot \bar{g}/\bar{\gamma}$ into (3.36) yields

$$\Delta g - \Delta \tilde{g} = 0.3086 \cdot H \cdot \left(\frac{\bar{\gamma} - \bar{g}}{\bar{\gamma}} \right) . \tag{3.38}$$

From (3.37) and (3.18) and setting the density ρ equal to $2.67 g/cm^3$, the difference between the mean normal gravity $\bar{\gamma}$ and the mean gravity $\bar{g}$ is:

$$\bar{\gamma} - \bar{g} = (\gamma_o - 0.1543 \cdot H^N) - (g + 0.0424 \cdot H) , \tag{3.39}$$

or

$$\bar{\gamma} - \bar{g} \doteq - (g + 0.1967 \cdot H - \gamma_o) , \tag{3.40}$$

where the factors 0.0424 and 0.1967 are also in mgal/m.

Because the Bouguer anomaly, denoted by Δg^B , is defined as the difference between the Bouguer gravity $g^B = g + 0.1967 \cdot H$ on the geoid and the normal gravity referred to the ellipsoid-- without taking into account the variation of the actual topography -- (Heiskanen and Moritz, 1967), the equation (3.40) can be written as:

$$\bar{\gamma} - \bar{g} \doteq - \Delta g^B . \tag{3.41}$$

Therefore, equation (3.38) becomes

$$\Delta g - \Delta \tilde{g} = - 0.3086 \cdot H \cdot \Delta g^B / \bar{\gamma} . \qquad (3.42)$$

The mean normal gravity $\bar{\gamma}$ can be replaced by the mean gravity γ_m on the ellipsoid. The relative error of this approximation is less than 1%. Substituting (3.42) into (3.35), we obtain finally (Vaníček and Krakiwsky, 1982):

$$\theta - \tilde{\theta} = \begin{Bmatrix} \xi \\ \eta \end{Bmatrix} - \begin{Bmatrix} \tilde{\xi} \\ \tilde{\eta} \end{Bmatrix} = \frac{-1}{4\pi\gamma_m} \iint_{\nu} \left(0.3086 \cdot H \cdot \frac{\Delta g^B}{\gamma_m} + \Delta G \right) \cdot \begin{Bmatrix} \cos\alpha \\ \sin\alpha \end{Bmatrix} \times \frac{dS(\psi)}{d\psi} \cdot d\nu + \frac{\Delta \tilde{g}}{\gamma_m} \cdot \begin{Bmatrix} \tan\beta_1 \\ \tan\beta_2 \end{Bmatrix} . \qquad (3.43)$$

For convenience, equation (3.43) is here called the Stokes-Molodenskij formula. In this equation, the contribution of the first term in the subintegral function may be regarded as the effect of the difference between the free-air anomalies on the geoid and those on the earth's surface on the plumb line curvature. The contribution of the second term may be regarded as the regional terrain and gravity effect on the curvature. The last term in (3.43) may be regarded as the north-south and east-west terrain profile effects (point effects) on the plumb line curvature. It is apparent that the Stokes-Molodenskij formula can compute the curvature effect of the plumb line more conveniently than Vening Meinesz's and Molodenskij's formulae together. The curvature effect of the plumb line, therefore, can be easily determined by combining the Stokes-

Molodenskij formula and the equation of the curvature effect of the normal plumb line.

CHAPTER 4

PRACTICAL EVALUATION OF THE STOKES-MOLODENSKIJ FORMULA

4.1 INTRODUCTION

The Stokes-Molodenskij formula requires the knowledge of the gravity anomaly $\Delta\tilde{g}$, and the normal height H^N for the solution of the terrain correction ΔG at any point on the surface of the earth. Practically, due to the discrete data for $\Delta\tilde{g}$ and H^N available, the formula (3.43) is evaluated as summations. The small element $d\mathcal{V}$ is replaced by an appropriate area element (compartment or block). A mean gravity anomaly and a mean normal height are necessarily computed for each compartment or block. Since the difference between the normal height and the orthometric height is fairly small, usually it does not exceed 0.1 m (Vaníček, 1974). In practice the former can be replaced by the latter without affecting the accuracy of the value ΔG.

For the computation of Stokes's integral, blocks of various sizes bounded by geographical grid lines $5^\circ \times 5^\circ$, $1^\circ \times 1^\circ$, $30' \times 30'$, $5' \times 5'$, and smaller are considered (Moritz, 1980b). In the neighborhood of the computation point, it is proper to use smaller blocks or compartments than for distant zones. For the Vening Meinesz integral, such blocks of a few sizes

can also be used. Because Vening Meinesz's integral has a stronger singularity than Stokes's integral, it requires more detailed representation of $\Delta\tilde{g}$ and more rigorous treatment around the computation point (Moritz, 1980b). Obviously, the integral in the Stokes-Molodenskij formula is similar to the Vening Meinesz integral so that the above applies to it too.

For the determination of the curvature effect of the plumb line by means of the Stokes-Molodenskij formula in this study, there are two different zones needed: innermost and inner (Fig.4.1). The reason for neglecting outer zone contribution to the curvature effect of the plumb line will be given later.

The innermost zone is chosen to be enclosed by a rectangle of the dimensions 9x7 km for $\Phi = 45^{\circ}$ (approximately 5x5 minute rectangle). It consists of 63 1x1 km blocks (Fig.4.2). In the central block around the computation point, circle-ring method is adopted for the central area contribution. The outer radius is equal to 564 m chosen on the basis of the same area as the central 1x1 km compartment. The inner zone covers an area of a 25x25 minute block around the computation point, excluding the innermost zone. It is subdivided into a few equal 5x5 minute cells. The choice of the boundary of the inner zone is discussed in Section 4.6.

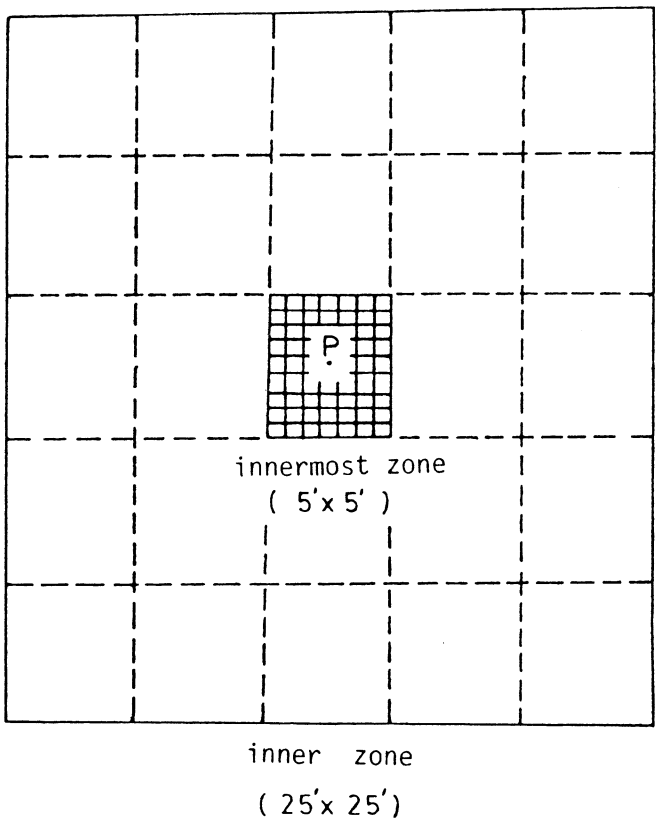

Figure 4.1: Innermost and inner zones.

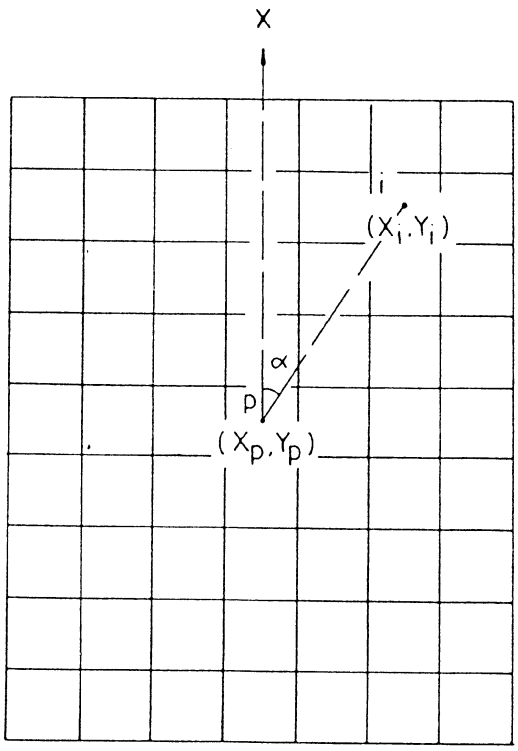

Figure 4.2: Innermost zone.

The choice of $5' \times 5'$ blocks is based on the fact that the mean gravity anomalies and the mean heights for these blocks are readily available. The data sets used for the numerical evaluation of the Stokes-Molodenskij formula include the point gravity anomalies, and the 5x5 minutes mean gravity anomalies and mean heights. The mean heights of 1x1 km blocks needed for the innermost zone are obtained from the topographic maps at the scale 1:50,000.

In the Stokes-Molodenskij formula, if the orthometric height is equal to 1000m, the first term in equation (3.43), $0.3086H\cdot\Delta g^{B}/\gamma_m$, is about 10^{-3} times smaller than the term Δg in Vening Meinesz's formula, equation (3.1). Besides, orthometric heights of almost 72% of the points in the world could be regarded as zero due to the fact that the about 72% of global area is covered with water. The contribution of the term to the plumb line curvature effect should be small. In order to exemplify the above reasoning, a few points in New Brunswick (NB) have been tested. The contributions are smaller than $0''.001$ everywhere. Therefore, the first term can be neglected. It could be said that the term makes no contribution to the curvature effect of the plumb line.

The numerical evaluation of the Stokes-Molodenskij formula is, therefore, integrated by a summation over discrete data:

$$\Delta\xi = \frac{-1}{4\pi\gamma_m}\sum \Delta G \cdot \frac{dS(\psi)}{d\psi}\cdot\cos\alpha\cdot\Delta\nu + \frac{\Delta\tilde{g}}{\gamma_m}\cdot\tan\beta_1$$

$$\Delta\eta = \frac{-1}{4\pi\gamma_m}\sum \Delta G \cdot \frac{dS(\psi)}{d\psi}\cdot\sin\alpha\cdot\Delta\nu + \frac{\Delta\tilde{g}}{\gamma_m}\cdot\tan\beta_2 \qquad (4.1)$$

and

$$\Delta G = \frac{R^2}{2\pi}\cdot\frac{\bar{H} - H_p}{s^3}\cdot\left(\Delta\tilde{g} + \frac{3\gamma}{2R}\cdot\zeta\right)\cdot\Delta\nu, \qquad (4.2)$$

where $\bar{H}$ is the mean height of the small compartment $\Delta\nu$. In equation (4.2), if the height anomaly ζ is unknown, it may be determined from satellite potential coefficients, i.e. Rapp 180 (Rapp, 1981). Because the value of $3\gamma/2R$ is small (approximately 0.23 mgal/m), if the value of $3\cdot\gamma/2R\cdot\zeta$ is smaller than the error of the gravity anomaly $\Delta\tilde{g}$, this term can be neglected. The height anomaly in the province of New Brunswick, the tested area, approximately ranges from -1 m to 2 m (Merry, 1975). This gives values of order of -0.2 to 0.5 mgal for $3\gamma/2R\cdot\zeta$. Then, equation (4.2) becomes

$$\Delta G = \frac{R^2}{2\pi}\cdot\frac{\bar{H} - H_p}{s^3}\cdot\Delta\tilde{g}\cdot\Delta\nu\ . \qquad (4.3)$$

Due to the fast growing denominator in equation (4.3), the value of ΔG will disappear very rapidly. For the outside of the inner zone, the contribution of ΔG is approximately equal to zero. A test of the contribution will be given in Section 4.6.

Therefore, the summation in equation (4.1) can be split into three parts, and the curvature effect components of the plumb line are given by:

$$\begin{aligned} \Delta\xi &= \Delta\xi_1 + \Delta\xi_2 + \Delta\xi_3 + \Delta\xi^N \\ \Delta\eta &= \Delta\eta_1 + \Delta\eta_2 + \Delta\eta_3 , \end{aligned} \tag{4.4}$$

where $\Delta\xi_1$ and $\Delta\xi_2$ are the contributions of the innermost and inner zones for the north-south component,

$\Delta\eta_1$ and $\Delta\eta_2$ are the contributions of the innermost and inner zones for the east-west component,

$\Delta\xi_3$ and $\Delta\eta_3$ are the north-south and the east-west terrain profile contributions to the curvature effect of the plumb line, respectively.

The terrain profile contributions are written as:

$$\begin{aligned} \Delta\xi_3 &= \frac{\Delta\tilde{g}}{\gamma_m}\cdot\tan\beta_1 \\ \Delta\eta_3 &= \frac{\Delta\tilde{g}}{\gamma_m}\cdot\tan\beta_2 . \end{aligned} \tag{4.5}$$

$\Delta\xi^N$ is the north-south component of the curvature effect of the normal plumb line.

4.2 PREDICTION OF MEAN GRAVITY ANOMALY

For the contribution of the innermost zone, the mean free-air and the mean Bouguer gravity anomalies of the 1x1 km blocks are computed from the point gravity data. The mean gravity anomaly, $\overline{\Delta g}$, for a region of area A, is given by (Heiskanen and Moritz, 1967):

$$\overline{\Delta g} = \frac{1}{A}\iint_A \Delta g \cdot dA \ , \tag{4.6}$$

where Δg is the point gravity anomaly. Because the blocks are small, there may not always be data available in the area. In order to determine the mean anomalies for such small areas, the point anomalies in those blocks can be predicted first, then the mean anomalies are determined by equation (4.6). There are several methods to predict the point anomalies, e.g. graphical interpolation from the gravity anomaly map, the least-squares surface fitting, the least-squares collocation, etc. Since the purpose of this thesis is not to determine an optimal value for the gravity anomaly, the most simple approach will be adopted: the least-squares surface fitting technique. This technique has been used successfully for a number of different purposes (Vaníček and Merry, 1973; Vaníček and Christodulides, 1974; Merry, 1975).

Since the Bouguer anomalies are always smooth enough for interpolation and extrapolation purposes, the prediction

of free-air anomalies is often performed through the intermediate step of Bouguer anomaly prediction (Sünkel and Kraiger, 1983).

In order to predict the 1x1 km mean anomalies within the innermost zone, all of the anomalies distributed within the zone are taken into account in the surface-fitting technique. For this technique, the Bouguer anomalies can be represented by an algebraic polynomial:

$$\Delta g^{B}(X,Y) = \sum_{j,k=o}^{n} a_{jk} \cdot X^{j} \cdot Y^{k} \quad . \tag{4.7}$$

The degree of the polynomial, n, will depend on the amount of data available and on the complexity of the surface desired. In general, a polynomial of second order is commonly used (Merry, 1975). The coefficients of this polynomial, a_{jk} ,are determined by using the least-squares fit to the Bouguer anomalies. The local coordinates (X,Y) are centred at an arbitrary point. The coordinates may be obtained from geodetic coordinates by means of the following equations:

$$\begin{aligned} X &= R(\Phi - \Phi_{o}) \\ Y &= R(\lambda - \lambda_{o}) \cdot \cos\Phi_{o} \quad , \end{aligned} \tag{4.8}$$

where (Φ, λ) are the geodetic latitude and longitude of the measured point,

(Φ_{o}, λ_{o}) are the coordinates of the arbitrary origin, and R is a mean radius of the earth.

After the coefficients a_{jk} and the covariance matrix C_a of the coefficients are obtained, the Bouguer anomaly Δg_i^B at the center of the i-th block and its standard deviation can be evaluated. The determinations of a_{jk}, C_a, Δg_i^B, and the standard deviation of the Bouguer anomaly are given in Appendix I.

On the basis of the polynomial of the second order used, the mean Bouguer anomaly $\overline{\Delta g}_i^B$ and mean free-air anomalies $\overline{\Delta g}_i$ for the i-th block are obtained from the following equations:

$$\overline{\Delta g}^B = \frac{1}{A} \cdot \iint_A \Delta g^B \cdot dA \quad . \tag{4.9}$$

Substituting (4.7) into (4.9) becomes

$$\overline{\Delta g}^B = \frac{1}{A} \sum_{j,k=o}^{2} a_{jk} \cdot \iint_A X^j \cdot Y^k \cdot dA \quad . \tag{4.10}$$

Integrating (4.10), if the origin (X_o, Y_o) is selected to coincide with the midpoint (X_i, Y_i) of the i-th block, we get (Appendix II):

$$\overline{\Delta g}^B(X_i, Y_i) = a_{00} + a_{02} \cdot \frac{s^2}{3} + a_{20} \cdot \frac{r^2}{3} + a_{22} \cdot \frac{r^2 s^2}{9} \quad , \tag{4.11}$$

where 2r, 2s are the north-south and east-west extents of the i-th block, respectively.

Because the free-air anomaly is given by (Heiskanen and Moritz, 1967):

$$\Delta g(X_i, Y_i) = \Delta g^B(X_i, Y_i) + 0.1119 \cdot H(X_i, Y_i) \quad , \tag{4.12}$$

where the factor 0.1119 is in mgal/m, the mean free-air anomaly is determined from:

$$\overline{\Delta g}(X_i, Y_i) = \frac{1}{A} \cdot \iint_A \Delta g^B \cdot dA + \frac{0.1119}{A} \cdot \iint_A H \cdot dA \quad . \tag{4.13}$$

Equation (4.13) can be hence written as:

$$\overline{\Delta g}(X_i, Y_i) = \overline{\Delta g}^B(X_i, Y_i) + 0.1119 \cdot \overline{H} \quad , \tag{4.14}$$

where

$$\overline{H} = \frac{1}{A} \cdot \iint_A H(X,Y) \cdot dA \quad . \tag{4.15}$$

Since it is difficult to know the function $H(X,Y)$, an alternate formula is:

$$\overline{H} = \frac{1}{n} \cdot \sum_{m=1}^{n} H_m \quad , \tag{4.16}$$

where n is the number of measured heights H at the block. The variance $\sigma^2_{\overline{H}}$ of the mean height is given by:

$$\sigma^2_{\overline{H}} = \frac{\sum_{m=1}^{n} (H_m - \overline{H})^2}{n - 1} \quad . \tag{4.17}$$

Equation (4.11) can be written in matrix form as:

$$\overline{\Delta g}^{B} = \underline{b} \cdot \underline{a}^{T} , \qquad (4.18)$$

where

$$\underline{a} = \left(a_{00}, a_{02}, a_{20}, a_{22} \right) ; \qquad \underline{b} = \left(b_1, b_2, b_3, b_4 \right),$$

and

$$b_1 = 1, \quad b_2 = s^2/3 , \quad b_3 = r^2/3 , \quad b_4 = r^2 s^2/9 . \qquad (4.19)$$

Then, applying the law of propagation of covariance (Vaníček, 1980), the variance of $\overline{\Delta g}^{B}$ is obtained from:

$$\sigma^2_{\overline{\Delta g}^{B}} = \underline{b} \cdot C_a \cdot \underline{b}^{T} . \qquad (4.20)$$

Assuming that the mean Bouguer anomaly is uncorrelated with the mean height, the variance of $\overline{\Delta g}$ is given by:

$$\sigma^2_{\overline{\Delta g}} = \sigma^2_{\overline{\Delta g}^{B}} + \left(0.1119 \cdot \sigma_{\overline{H}}\right)^2 . \qquad (4.21)$$

4.3 INNERMOST ZONE CONTRIBUTION

In the vicinity of the computation point, Vening Meinesz's function is approximated by (Heiskanen and Moritz, 1967):

$$\frac{dS(\psi)}{d\psi} \doteq -\frac{2}{\psi^2} . \qquad (4.22)$$

The relative error of this approximation is about 1% for the linear distance s=10 km from the computation point, and about 3% for s=30 km (ibid., p.121). Within the small

spherical distance Ψ (corresponding to a linear distance of a few kilometres), we may regard the sphere as a plane, where Ψ is given by:

$$\Psi \doteq s/R \ . \tag{4.23}$$

Substituting (4.23) into (4.22) yields:

$$\frac{dS(\Psi)}{d\Psi} \doteq -\frac{2R^2}{s^2} \ . \tag{4.24}$$

The solid angle element $d\nu$ in the rectangular coordinate system and in the polar coordinate system are written respectively as:

$$d\nu = \frac{dx \cdot dy}{R^2} \tag{4.25}$$

and

$$d\nu = \frac{s \cdot ds \cdot d\alpha}{R^2} \ . \tag{4.26}$$

Substituting (4.24) and (4.25) into (3.43), the contribution of the innermost zone to the curvature effect components is:

$$\begin{aligned} \Delta\xi_1 &= \frac{-1}{4\pi\gamma_m} \iint_{A_1} \Delta G \cdot \frac{-2R^2}{s^2} \cdot \cos\alpha \cdot \frac{dx \cdot dy}{R^2} \\ \Delta\eta_1 &= \frac{-1}{4\pi\gamma_m} \iint_{A_1} \Delta G \cdot \frac{-2R^2}{s^2} \cdot \sin\alpha \cdot \frac{dx \cdot dy}{R^2} \ . \end{aligned} \tag{4.27}$$

Rearranging (4.27) yields:

$$\begin{aligned} \Delta\xi_1 &= \frac{1}{2\pi\gamma_m} \iint_{A_1} \Delta G \cdot \frac{\cos\alpha}{s^2} \cdot dx \cdot dy \\ \Delta\eta_1 &= \frac{1}{2\pi\gamma_m} \iint_{A_1} \Delta G \cdot \frac{\sin\alpha}{s^2} \cdot dx \cdot dy \end{aligned} \tag{4.28}$$

and (cf. equation (3.6))

$$\Delta G = \frac{1}{2\pi} \iint_{\Delta A_1} \frac{H - H_p}{s^3} \cdot \Delta\tilde{g} \cdot dx \cdot dy \ , \tag{4.29}$$

where ΔA_1 is the area of the 1x1 km block inside the innermost zone. Therefore, the part of equation (4.1) pertinent to the innermost zone is given by:

$$\begin{aligned} \Delta\xi_{1,1} &= \frac{1}{2\pi\gamma_m} \sum_{i=1}^{nl} \Delta G_i \cdot \cos\alpha_i \cdot \left(\frac{\Delta x \cdot \Delta y}{s^2}\right)_i \\ \Delta\eta_{1,1} &= \frac{1}{2\pi\gamma_m} \sum_{i=1}^{nl} \Delta G_i \cdot \sin\alpha_i \cdot \left(\frac{\Delta x \cdot \Delta y}{s^2}\right)_i \end{aligned} \tag{4.30}$$

and

$$\Delta G_i = \frac{1}{2\pi} \cdot (\bar{H}_i - H_p) \cdot \overline{\Delta g}_i \cdot \left(\frac{\Delta x \cdot \Delta y}{s^3}\right)_i \tag{4.31}$$

$$\Delta A_1 = \Delta x \cdot \Delta y \ , \tag{4.32}$$

where nl is the number of 1x1 km blocks used,

$\bar{H}_i$ is the mean value of the height in the i-th block,

$\overline{\Delta g}_i$ is the mean value in the i-th block of the free-air anomaly,

α_i is the azimuth of the line connecting the computation point and the midpoint of the i-th block,

$\Delta x = \Delta y = 1$ km,

s is the distance between the computation point and the midpoint of the i-th block, and

α_i, s are given by:

$$\alpha_i = \arctan\left(\frac{Y_i - Y_p}{X_i - X_p}\right) \tag{4.33}$$

$$s = \sqrt{(X_i - X_p)^2 + (Y_i - Y_p)^2}, \tag{4.34}$$

where (X_p, Y_p) are the coordinates of the computation point, and (X_i, Y_i) are the coordinates of the midpoint of the i-th block in a local plane coordinate system (Fig.4.2).

For the 1x1 km blocks near the computation point, in equations (4.30), it is not accurate enough to evaluate the values of $\Delta x \cdot \Delta y / s^2$ and $\Delta x \cdot \Delta y / s^3$ at the center of each block. A more rigorous approach is to integrate over the block. Setting $C = \Delta x \cdot \Delta y / s^2$ and $D = \Delta x \cdot \Delta y / s^3$, the more proper values of C and D are given by:

$$\begin{aligned} \bar{C} &= \frac{1}{\Delta A_i} \iint_{\Delta A_i} C \cdot dA \\ \bar{D} &= \frac{1}{\Delta A_i} \iint_{\Delta A_i} D \cdot dA , \end{aligned} \tag{4.35}$$

where $\bar{C}$ and $\bar{D}$ denote the mean values of C and D for the block, and ΔA_i is the block area.

The error in the numerical integration is illustrated in Table 4.1.

For those blocks within a rectangular region of the dimensions 7x7 km, centred on the computation point, the mean values (4.35) are used. The relative error is thus kept below 1.8% for C and 4% for D.

TABLE 4.1

The differences between the values C and D and their mean values.

dist.	C	$\bar{C}$	error	D	$\bar{D}$	error
(s)			(%)			(%)
1 km	1.00E+0	1.16E+0	13.9	1.00E-3	1.40E-3	28.7
2 km	2.50E-1	2.60E-1	4.0	1.25E-4	1.37E-4	8.8
3 km	1.11E-1	1.13E-1	1.8	3.70E-5	3.86E-5	4.0
4 km	6.25E-2	6.31E-2	1.0	1.56E-5	1.60E-5	2.3
5 km	4.00E-2	4.03E-2	0.7	8.00E-6	8.12E-5	1.5

For the central block where the computation point lies, since the midpoint of the block coincides with the computation point, equations (4.30) cannot be used to evaluate the contribution of the central block. For this reason, the circular-ring method is adopted. In this study, there are three rings used whose radii are 100m, 200m, and 564m (Fig.4.3). The outer radius is chosen on the basis of the same area as the central compartment, therefore the total area of 4 corners is equal to the total area of 4 overlaps (Fig.4.3). It is assumed that the contributions of the corners and the overlaps are balanced out.

Substituting (4.24) and (4.26) into (3.43), we obtain

$$\Delta\xi_1 = \frac{-1}{4\pi\gamma_m}\iint_{A_2}\Delta G\cdot\frac{-2R^2}{s^2}\cdot\cos\alpha\cdot\frac{s\cdot ds\cdot d\alpha}{R^2}$$

$$\Delta\eta_1 = \frac{-1}{4\pi\gamma_m}\iint_{A_2}\Delta G\cdot\frac{-2R^2}{s^2}\cdot\sin\alpha\cdot\frac{s\cdot ds\cdot d\alpha}{R^2} \qquad (4.36)$$

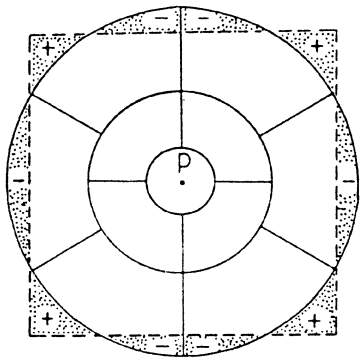

Figure 4.3: Circular-ring compartments.

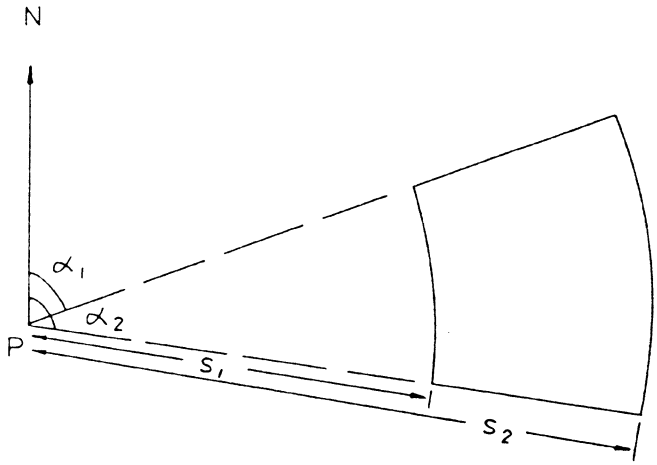

Figure 4.4: A template compartment.

and

$$\Delta G = \frac{R^2}{2\pi}\iint_{\Delta A_2} \frac{H - H_p}{s^3}\cdot\Delta\tilde{g}\cdot\frac{s\cdot ds\cdot d\alpha}{R^2} \quad , \tag{4.37}$$

where A_2 is the central block area, and

ΔA_2 is the area of the circular-ring compartment.

Rearranging equations (4.36) and (4.37), we obtain

$$\begin{aligned} \Delta\xi_1 &= \frac{1}{2\pi\gamma_m}\iint_{A_2}\Delta G\cdot\frac{\cos\alpha}{s}\cdot ds\cdot d\alpha \\ \Delta\eta_1 &= \frac{1}{2\pi\gamma_m}\iint_{A_2}\Delta G\cdot\frac{\sin\alpha}{s}\cdot ds\cdot d\alpha \end{aligned} \tag{4.38}$$

and

$$\Delta G = \frac{1}{2\pi}\iint_{\Delta A_2}\frac{H - H_p}{s^2}\cdot\Delta\tilde{g}\cdot ds\cdot d\alpha \quad . \tag{4.39}$$

Then performing these integrations, the contribution of the central block is given by (Appendix III):

$$\begin{aligned} \Delta\xi_{1,2} &= \frac{1}{2\pi\gamma_m}\cdot\sum_{j=1}^{m}\Delta G_j\cdot(\sin\alpha_2 - \sin\alpha_1)\cdot\ln(s_2/s_1) \\ \Delta\eta_{1,2} &= \frac{1}{2\pi\gamma_m}\cdot\sum_{j=1}^{m}\Delta G_j\cdot(\cos\alpha_1 - \cos\alpha_2)\cdot\ln(s_2/s_1) \end{aligned} \tag{4.40}$$

and

$$\Delta G_j = \frac{1}{2\pi}\cdot(\alpha_2 - \alpha_1)\cdot(\bar{H}_j - H_p)\cdot\overline{\Delta g}_j\cdot\left(\frac{1}{s_1} - \frac{1}{s_2}\right) \quad , \tag{4.41}$$

where $\bar{H}_j$ is the mean height of the j-th compartment,

α_1, α_2 are the azimuths of two edges of the compartment, respectively, and $\alpha_2 > \alpha_1$ (Fig.4.4),

s_1 , s_2 are the inner and outer radii,

$\overline{\Delta g}_j$ is the mean free-air anomaly, and

m is the number of the compartments used (within the circular rings).

Finally, the total contribution of the innermost zone is obtained from:

$$\begin{aligned} \Delta\xi_1 &= \Delta\xi_{1,1} + \Delta\xi_{1,2} \\ \Delta\eta_1 &= \Delta\eta_{1,1} + \Delta\eta_{1,2} \end{aligned} \quad . \tag{4.42}$$

4.4 INNER ZONE CONTRIBUTION

The inner zone, composed of a number of 5x5 minutes blocks, covers an area of a 25x25 minute geographic rectangle, excluding the innermost zone. Analogous to (4.30) and (4.31), the contribution of the inner zone can be written as (cf. equation 4.1):

$$\begin{aligned} \Delta\xi_2 &= \frac{-1}{4\pi\gamma_m} \sum_{i=1}^{n2} \Delta G_i \cdot \left(\frac{dS(\psi)}{d\psi}\right)_i \cdot \cos\phi_i \cdot \cos\alpha_i \cdot \Delta\phi \cdot \Delta\lambda \\ \Delta\eta_2 &= \frac{-1}{4\pi\gamma_m} \sum_{i=1}^{n2} \Delta G_i \cdot \left(\frac{dS(\psi)}{d\psi}\right)_i \cdot \cos\phi_i \cdot \sin\alpha_i \cdot \Delta\phi \cdot \Delta\lambda \end{aligned} \tag{4.43}$$

and

$$\Delta G_i = \frac{R^2}{2\pi} \cdot \frac{(\bar{H}_i - H_p)}{s^3} \overline{\Delta g}_i \cdot \cos\phi_i \cdot \Delta\phi \cdot \Delta\lambda \ , \tag{4.44}$$

$$s = 2R\sin(\psi/2) \ , \tag{4.45}$$

where n2 is the number of 5'x5' blocks used,

ϕ_i is the latitude of the midpoint of the i-th block,

$\Delta\phi = \Delta\lambda = 5'$,

and the other symbols have the same meaning as before.

In the above equations, ψ_i , α_i are given by:

$$\psi_i = \arccos(\sin\phi_p \cdot \sin\phi_i + \cos\phi_p \cdot \cos\phi_i \cdot \cos(\lambda_i - \lambda_p)) \qquad (4.46)$$

$$\alpha_i = \arctan\left(\frac{\cos\phi_i \sin(\lambda_i - \lambda_p)}{\cos\phi_p \cdot \sin\phi_i - \sin\phi_p \cdot \cos\phi_i \cdot \cos(\lambda_i - \lambda_p)} \right), \qquad (4.47)$$

where (ϕ_p, λ_p) are the geodetic coordinates of the computation point, and (ϕ_i, λ_i) are the geodetic coordinates of the midpoint of the i-th block.

Due to the rapid change in Vening Meinesz's function, it should be treated rigorously

$$\overline{\frac{dS(\psi)}{d\psi}} = \frac{1}{A}\iint_A \frac{dS(\psi)}{d\psi} \cdot dA \ , \qquad (4.48)$$

where $\overline{dS(\psi)/d\psi}$ denotes the mean value of $dS(\psi)/d\psi$ for the block, and A is the block area. For those blocks whose spherical distance from the computation point is smaller than $0^{\circ}.5$, the value of $dS(\psi)/d\psi$ is replaced by the mean value of $\overline{dS(\psi)/d\psi}$ (Merry, 1975).

Analogously, the mean value of $R^2 \cdot \cos\phi \cdot \Delta\phi \cdot \Delta\lambda / s^3$ in (4.44) is given by:

$$E = \frac{1}{\Delta A}\iint_{\Delta A} \frac{R^2 \cdot \cos\phi \cdot \Delta\phi \cdot \Delta\lambda}{s^3} \cdot dA \ , \qquad (4.49)$$

where ΔA is the $5' \times 5'$ block area. Since $\Delta A = R^2 \cdot \cos\phi \cdot \Delta\phi \cdot \Delta\lambda$, equation (4.49) may be written as:

$$E = \iint_{\Delta A} \frac{1}{s^3} \cdot dA \quad . \tag{4.50}$$

Equation (4.50) is used when the spherical distance of those blocks is smaller than 15'. The relative error will be below 4%.

4.5 TERRAIN PROFILE CONTRIBUTION

The terrain profile contribution to the components of the curvature effect are given by equation (4.5). These can attain large values in steep mountains. For the terrain profile contribution, sometimes the uncertainties of the terrain inclination will give large error for the curvature. For the small terrain inclination, between 0° and 25°, the error of 1° in β value will give the error of 0".004/mgal for the plumb line curvature effect. For instance, when the free-air anomaly is 50 mgals, the error of the curvature effect is 0".2. No matter how the terrain inclinations are measured, either from topographic maps or from field works, the evaluation of the inclinations should be performed carefully.

4.5.1 Evaluation of terrain slope

The evaluation of terrain slope can be done simply. Let the north-south (or east-west) terrain profile be a function of horizontal coordinate x (or y). Then we may write the north-south and east-west terrain profiles, denoted by H(x) and H(y) respectively:

$$H(x) = \sum_{i=0}^{u} c_i \cdot x^i$$
$$H(y) = \sum_{i=0}^{u} d_i \cdot y^i \quad , \tag{4.51}$$

where c_i , d_i are some coefficients, u is the number of coefficients, and (x,y) are the coordinates referred to the local system, whose origin coincides with the computation point P. Measuring the heights H(x) and H(y) for several values x and y, the coefficients c_i and d_i can be determined using the least-squares procedure. The north-south and east-west terrain slopes are given by the coefficients c_1 and d_1 .

This simple model has been tested in two different kinds of areas, flat and hilly. Twenty one data for each profile are measured at the following coordinates: -250m, -200m,...., 200m, 250m, in 25m interval. The results are shown in Tables 4.2 and 4.3. As can be seen, the number of the coefficients does not make significant difference for the terrain profile contribution in flat area. However, the significant difference is demonstrated in hilly area. In this case, the choice of the number of the coefficients comes into question.

Therefore, another approach to estimate the terrain slope is developed. Fig.4.5 shows the north-south terrain profile at the computation point. Let us choose points P_2 and P_1 to be north and south of the computation point P,

TABLE 4.2

Terrain profile contribution in flat area.

Number of coefficient	N − S component	standard deviation	E − W component	standard deviation
	"	"	"	"
3	-0.016	0.003	0.032	0.003
4	-0.043	0.001	0.013	0.005
5	-0.043	0.001	0.013	0.002
6	-0.044	0.002	0.019	0.003
7	-0.044	0.002	0.019	0.003
8	-0.043	0.003	0.017	0.005

TABLE 4.3

Terrain profile contribution in hilly area.

Number of coefficient	N − S component	standard deviation	E − W component	standard deviation
	"	"	"	"
3	0.758	0.058	0.428	0.085
4	0.820	0.149	0.709	0.207
5	0.820	0.088	0.709	0.121
6	0.918	0.159	0.915	0.213
7	0.918	0.120	0.915	0.140
8	1.063	0.187	1.145	0.210

respectively. In Fig.4.5, H_2 and H_1 are the heights of the points P_2 and P_1. Therefore, the terrain slope can be determined from:

$$\tan \beta_1 = \frac{\Delta H}{2r}, \qquad (4.52)$$

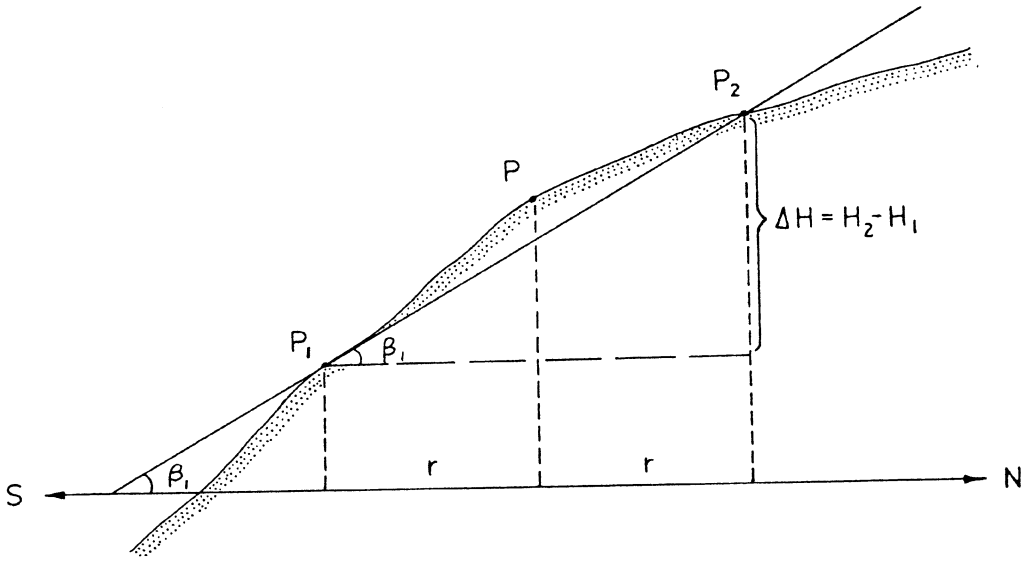

Figure 4.5: North-south terrain profile at computation point.

where r is the distance from the computation point P. Then the terrain profile contribution to the curvature effect of the plumb line is determined using (4.52) and (4.5). Since the tangent of β_1 is a very localized parameter, if we choose 10 different values of r and compute the terrain slopes and the curvature effects, the results are different (Tables 4.4 and 4.5). In flat area, maximum difference between the curvature effects determined from different distances is about 0".015 (Table 4.4). In hilly area, maximum difference reaches about 1".2 (Table 4.5). In this case, it may be necessary that the the least-squares approximation be used to find a trend for the terrain slope.

In order to determine a trend for the terrain slope, the terrain slope $\tan\beta_1$ can be represented by an algebraic polynomial of r:

$$\tan\beta_1(r) = \sum_{i=0}^{2} a_i \cdot r^i , \qquad (4.53)$$

where a_i are some coefficients. The coefficients can be determined using the least-squares approximation. When the distance r approaches to zero, the coefficient a_o is the estimated value for the terrain slope at the point of computation (Fig.4.6).

For the determination of the coefficients and covariance matrix of the coefficients see Appendix I. The variance of $\tan\beta_1$ is equal to $\sigma^2_{a_o}$. The determination of the

TABLE 4.4

Terrain profile contributions referred to different distances r in a flat area.

distance r	N – S component		E – W component	
	terrain slope	curvature effect	terrain slope	curvature effect
		"		"
25 m	0.009	– 0.044	– 0.004	0.022
50 m	0.010	– 0.049	– 0.004	0.022
75 m	0.008	– 0.040	– 0.003	0.016
100 m	0.008	– 0.040	– 0.002	0.012
125 m	0.007	– 0.035	– 0.004	0.022
150 m	0.008	– 0.040	– 0.005	0.024
175 m	0.007	– 0.035	– 0.004	0.022
200 m	0.007	– 0.035	– 0.004	0.022
225 m	0.007	– 0.035	– 0.004	0.022
250 m	0.006	– 0.031	– 0.003	0.016

TABLE 4.5

Terrain profile contributions referred to different distances r in a hilly area.

distance r	N – S component		E – W component	
	terrain slope	curvature effect	terrain slope	curvature effect
		"		"
25 m	0.323	1.403	0.408	1.774
50 m	0.251	1.092	0.213	0.927
75 m	0.236	1.026	0.274	1.192
100 m	0.229	0.993	0.305	1.324
125 m	0.219	0.953	0.226	0.980
150 m	0.213	0.927	0.173	0.750
175 m	0.198	0.860	0.170	0.738
200 m	0.187	0.811	0.168	0.728
225 m	0.186	0.809	0.148	0.632
250 m	0.186	0.809	0.128	0.556

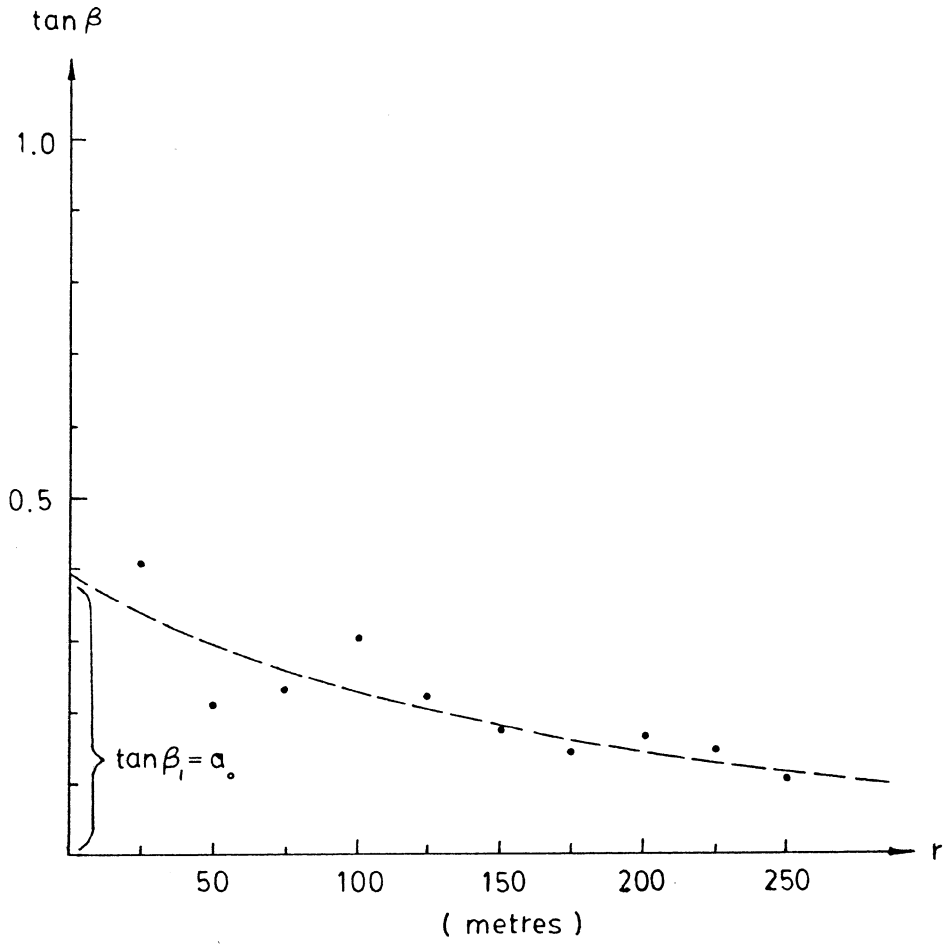

Figure 4.6: A trend for the terrain slope.

east-west terrain inclination follows the same computational procedures as that of the north-south.

4.6 ZONE BOUNDARY FOR THE CONTRIBUTION OF THE REGIONAL TERRAIN AND GRAVITY EFFECTS

It has been already stated in Section 4.1 that the value of ΔG disapears very rapidly with distance because of the fast growing denominator in the subintegral function. Thus, the integration does not have to be carried out very far.

In order to determine zone boundary for the contribution of ΔG (regional terrain and gravity effect) the variation of the geographic rectangle ranges from $15'x15'$ to $1^{\circ}05'x1^{\circ}05'$, in $10'$ increments. Computing the contributions of the values ΔG to the curvature effect and their RMS and taking the values of $1^{\circ}05'x1^{\circ}05'$ as standard, the differences in the curvature effects and the RMS from the standards are shown in Fig.4.7. The tested area is chosen in a hilly area whose heights range from 15m to 480m. From the figure, a conspicuous change in the differences occurs at $25'x25'$ on this graph: it appears that the contribution of ΔG to the curvature effect of the plumb line converges at this size of the zone. The contribution coming from the value ΔG may be regarded as the regional terrain and gravity effect on the curvature of the plumb line, Consequently, it can be concluded that topography and gravity outside the above zone make no effect.

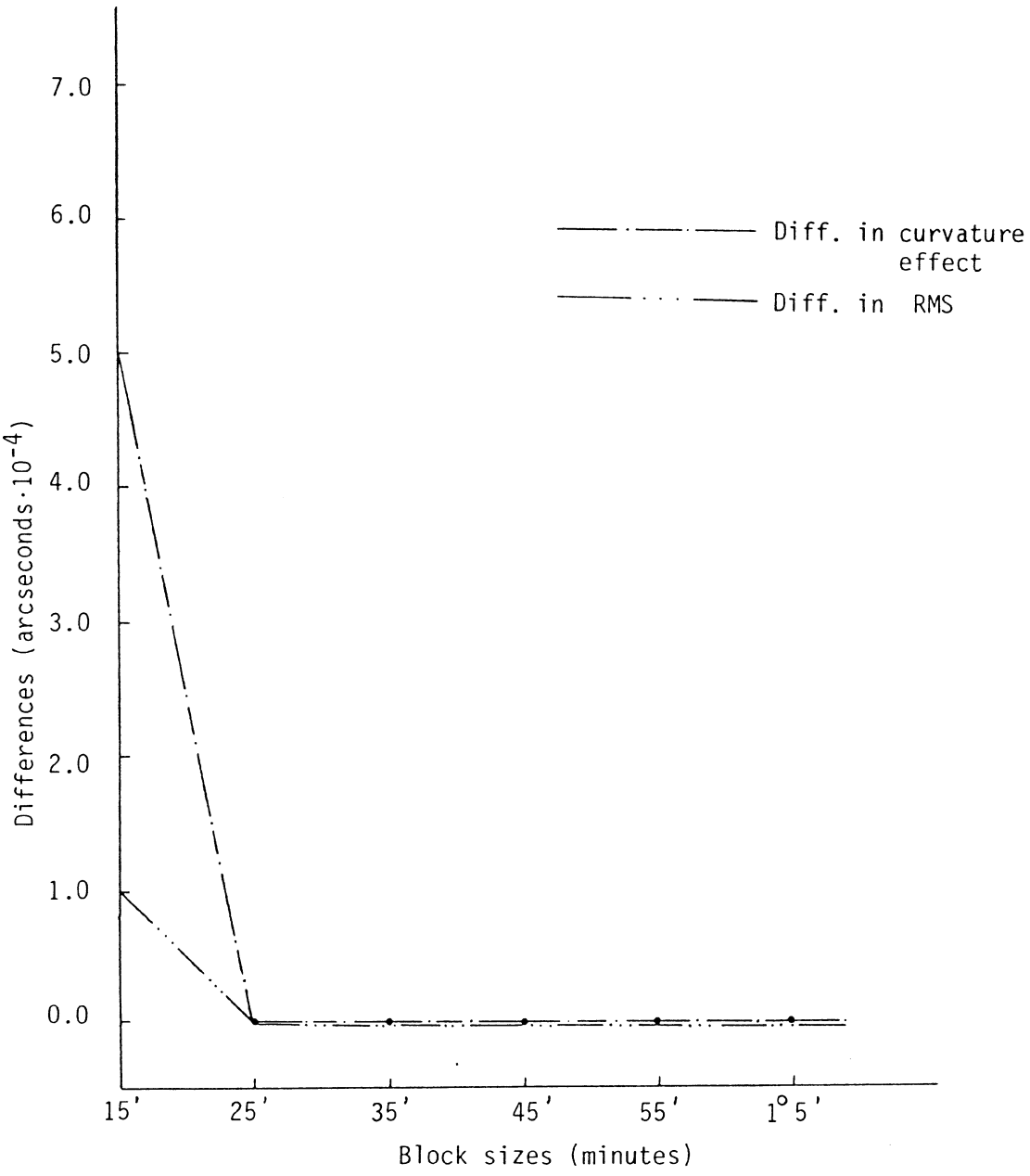

Figure 4.7: Zone boundary for the contribution of ΔG.

4.7 ESTIMATES OF ACCURACY

In order to examine the reliability of the results, the accuracy of the curvature effect of the plumb line has to be estimated. The uncertainties of the plumb line curvature effect are propagated from the errors of the gravity anomalies and the heights. The gravity anomalies are correlated with each other as a function of distance (Heiskanen and Moritz, 1967). The representation of this correlation can be carried out empirically (Lachapelle and Schwarz, 1980). The mean gravity anomalies are also correlated with each other. In this thesis, for the accuracy estimation of the curvature effect, the mean gravity anomalies are assumed to be uncorrelated. On the basis of this assumption, from equations (4.4), the standard deviations of the components of the curvature effect are determined from:

$$\begin{aligned} \sigma_{\Delta\xi} &= \sqrt{(\sigma^2_{\Delta\xi_1} + \sigma^2_{\Delta\xi_2} + \sigma^2_{\Delta\xi_3})} \\ \sigma_{\Delta\eta} &= \sqrt{(\sigma^2_{\Delta\eta_1} + \sigma^2_{\Delta\eta_2} + \sigma^2_{\Delta\eta_3})} \,. \end{aligned} \tag{4.54}$$

and the variances of the curvature components of the innermost zone are obtained from:

$$\begin{aligned} \sigma^2_{\Delta\xi_1} &= \sigma^2_{\Delta\xi_{1,1}} + \sigma^2_{\Delta\xi_{1,2}} \\ \sigma^2_{\Delta\eta_1} &= \sigma^2_{\Delta\eta_{1,1}} + \sigma^2_{\Delta\eta_{1,2}} \end{aligned} \tag{4.55}$$

The terms in (4.54) and (4.55) are determined from the following expressions (cf. (4.5), (4.31), (4.40), and (4.43)):

$$
\begin{aligned}
\sigma_{\Delta\xi_{1,1}} &= \frac{1}{2\pi\gamma_m}\sqrt{\sum_{i=1}^{n1}\{\cos\alpha_i\cdot C_i\cdot\sigma_{\Delta G_i}\}^2} \\
\sigma_{\Delta\xi_{1,2}} &= \frac{1}{2\pi\gamma_m}\sqrt{\sum_{i=1}^{m}\{(\sin\alpha_2-\sin\alpha_1)\cdot\ln(s_2/s_1)\cdot\sigma_{\Delta G_i}\}^2} \\
\sigma_{\Delta\xi_2} &= \frac{1}{2\pi\gamma_m}\sqrt{\sum_{j=1}^{n2}\{\frac{dS(\Psi)}{d\Psi}\cdot\cos\alpha_j\cdot\cos\phi_j\cdot\Delta\Phi\cdot\Delta\lambda\cdot\sigma_{\Delta G_j}\}^2} \\
\sigma_{\Delta\xi_3} &= \frac{1}{\gamma_m}\sqrt{\{(\tan\beta_1\cdot\sigma_{\Delta\tilde{g}})^2+(\Delta\tilde{g}\cdot\sigma_{\tan\beta_1})^2\}}
\end{aligned}
\qquad (4.56)
$$

$$
\begin{aligned}
\sigma_{\Delta\eta_{1,1}} &= \frac{1}{2\pi\gamma_m}\sqrt{\sum_{i=1}^{n1}\{\sin\alpha_i\cdot C_i\cdot\sigma_{\Delta G_i}\}^2} \\
\sigma_{\Delta\eta_{1,2}} &= \frac{1}{2\pi\gamma_m}\sqrt{\sum_{i=1}^{m}\{(\cos\alpha_1-\cos\alpha_2)\cdot\ln(s_2/s_1)\cdot\sigma_{\Delta G_i}\}^2} \\
\sigma_{\Delta\eta_2} &= \frac{1}{2\pi\gamma_m}\sqrt{\sum_{j=1}^{n2}\{\frac{dS(\Psi)}{d\Psi}\cdot\sin\alpha_j\cdot\cos\phi_j\cdot\Delta\Phi\cdot\Delta\lambda\cdot\sigma_{\Delta G_j}\}^2} \\
\sigma_{\Delta\eta_3} &= \frac{1}{\gamma_m}\sqrt{\{(\tan\beta_2\cdot\sigma_{\Delta\tilde{g}})^2+(\Delta\tilde{g}\cdot\sigma_{\tan\beta_2})^2\}} ,
\end{aligned}
$$

where n1 is the number of the 1x1 km blocks used,

m is the number of compartments within the circular rings used, and

n2 is the number of the 5'x5' blocks used.

The other symbols have been described in the preceding sections.

By estimating all of the standard deviations in (4.56), we obtained the values shown in Table 4.6. The error budget for the values is based on the assumptions that the standard deviations of the 1x1 km block mean gravity anomalies and mean heights are 2 mgals and 5 metres for flat areas and 5 mgals and 15 metres for hilly areas, and that the standard deviations of the 5'x5' mean gravity anomalies and mean heights are 10 mgals and 25 metres for both flat and hilly areas. From Table 4.6, depending on the accuracy required, some of the values can be neglected.

TABLE 4.6

Error budget for all of the values in (4.56).

0".0001	<	$\sigma_{\Delta\xi_2}$	,	$\sigma_{\Delta\eta_2}$	< 0".005
0".001	<	$\sigma_{\Delta\xi_{1,1}}$, $\sigma_{\Delta\xi_{1,2}}$, $\sigma_{\Delta\eta_{1,1}}$, $\sigma_{\Delta\eta_{1,2}}$			< 0".05
0".001	<	$\sigma_{\Delta\xi_3}$	,	$\sigma_{\Delta\eta_3}$	< 0".3

CHAPTER 5

COMPUTATIONAL RESULTS AND COMPARISONS

5.1 COMPUTATIONAL RESULTS

Six test stations located in the province of New Brunswick (Fig.5.1) have been selected for this thesis. Their geodetic coordinates and elevations are shown in Tables 5.1 through 5.6. Two of them, stations 2 and 3, lie in mountainous areas, the rest in flat areas.

In Tables 5.1 through 5.6, the results are shown from the technique based on the combination of Stokes's and Molodenskij's approaches. The data used have been described above. For convenience, the curvature effect of the plumb line obtained from the Stokes-Molodenskij formula is here called the Stokes-Molodenskij curvature effect, abbreviated by S-M. In the Tables, the first two rows show the contributions of ΔG of the innermost and inner zones. Row 3 shows the terrain profile contributions. The meanings of the rest of the rows can be easily interpreted from the Tables.

The contributions of ΔG are larger in mountainous areas than in flat areas. The maximum value for the contributions is 0.1 in all of the tested points. Among the contributions, the terrain profile contributions along the

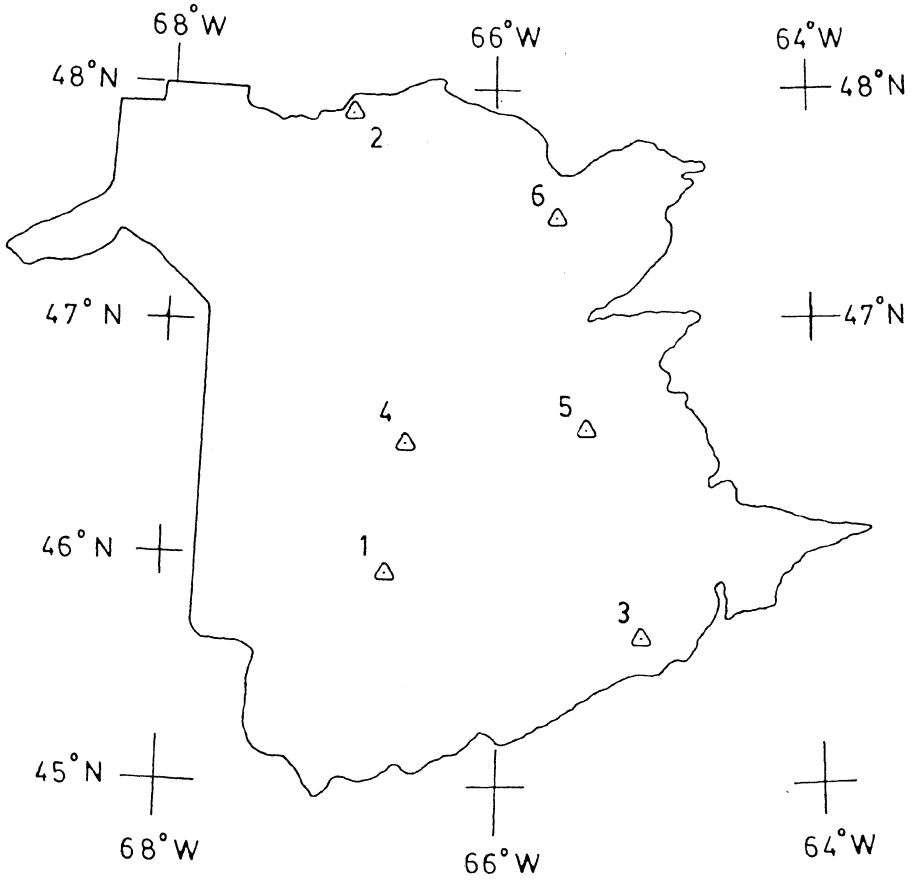

Figure 5.1: Distribution of the tested stations in New Brunswick.

TABLE 5.1

The Stokes-Molodenskij curvature effect at station 1.

Station # 1

Latitude = 45-57-42.85
Longitude = 293-21-42.32
Height = 10.8 M

Unit: arcseconds

		N - S comp.	Standard deviation	E - W comp.	Standard deviation
Inner-most zone	CONTRIBUTION	- 0.01	0.01	0.01	0.01
Inner zone		0.00	0.00	0.00	0.00
Point N $\Delta\theta$		- 0.05 0.00	0.00	0.02	0.00
Curvature effect		- 0.06	0.01	0.03	0.01

TABLE 5.2

The Stokes-Molodenskij curvature effect at station 2.

Station # 2 Unit: arcseconds		Latitude = 47-52-55.29 Longitude = 293-06-48.78 Height = 483.1 M		
	N - S comp.	Standard deviation	E - W comp.	Standard deviation
CONTRIBUTION Inner-most zone	− 0.01	0.01	0.02	0.00
Inner zone	0.00	0.00	− 0.03	0.00
Point	1.44	0.11	1.71	0.27
N Δθ	− 0.08			
Curvature effect	1.35	0.11	1.70	0.27

TABLE 5.3

The Stokes-Molodenskij curvature effect at station 3.

Station # 3 Unit: arcseconds		Latitude = 45-44-21.18 Longitude = 294-51-05.51 Height = 381.4 M		
	N - S comp.	Standard deviation	E - W comp.	Standard deviation
CONTRIBUTION Inner-most zone	0.11	0.02	− 0.02	0.02
Inner zone	− 0.01	0.00	0.01	0.00
Point N $\Delta\theta$	1.06 − 0.06	0.10	0.19	0.04
Curvature effect	1.10	0.10	0.18	0.04

TABLE 5.4

The Stokes-Molodenskij curvature effect at station 4.

Station # 4 Unit: arcseconds			Latitude = 46-26-59.54 Longitude = 293-28-33.69 Height = 235.2 M	
	N - S comp.	Standard deviation	E - W comp.	Standard deviation
Inner-most zone	CONTRIBUTION			
	− 0.00	0.00	0.00	0.00
Inner zone				
	0.00	0.00	0.00	0.00
Point N				
	− 0.04	0.05	0.04	0.01
$\Delta\theta$				
	− 0.04			
Curvature effect				
	− 0.08	0.05	0.04	0.01

TABLE 5.5

The Stokes-Molodenskij curvature effect at station 5.

Station # 5 Unit: arcseconds		Latitude = 46-43-55.46 Longitude = 294-34-22.97 Height = 93.6 M		
		N - S comp.	Standard deviation	E - W comp.	Standard deviation
CONTRIBUTION	Inner-most zone	0.00	0.00	0.00	0.00
	Inner zone	0.00	0.00	0.00	0.00
	Point	− 0.01	0.00	− 0.01	0.00
	N $\Delta\theta$	− 0.02			
Curvature effect		− 0.03	0.00	− 0.01	0.00

TABLE 5.6

The Stokes-Molodenskij curvature effect at station 6.

Station # 6 Unit: arcseconds		Latitude = 47-37-15.39 Longitude = 294-20-44.91 Height = 9.1 M		
		N - S comp.	Standard deviation	E - W comp.	Standard deviation
Inner-most zone	CONTRIBUTION	0.01	0.01	0.00	0.01
Inner zone		0.00	0.00	0.02	0.00
Point		0.07	0.04	− 0.05	0.01
N Δθ		0.00			
Curvature effect		0.08	0.04	− 0.03	0.01

north-south and the east-west directions are a lot larger than the others. The east-west terrain profile contribution to the plumb line curvature effect reaches about 1".7 (at station 2).

5.2 COMPARISONS BETWEEN THE STOKES-MOLODENSKIJ AND THE ASTRO-GRAVIMETRIC CURVATURE EFFECTS.

Equation (3.27) indicates that if the geoidal and the surface deflections (or astro-geodetic deflection) are known, then the curvature effect of the plumb line can be determined. For convenience, the curvature effect of the plumb line obtained from the difference between the geoidal deflection and the surface deflection is here called the astro-gravimetric curvature effect, abbreviated by A-G.

Both the surface and geoidal deflections are available for the tested points. The geoidal deflections are predicted by program GDOVE, written by Lachapelle (Table 5.7); the surface deflections (Canadian Astro-geodetic deflections, 1981) are available from Geodetic Survey of Canada. If the surface deflections and the geoidal deflections are referred to different ellipsoids, this two kinds of deflections must be brought into the same system. That must be done before determining the curvature effect.

The surface deflections refer to a geocentric ellipsoid with parameters (F.Faucher, personal communication, 1984):

$$a = 6378135 \text{ metres}$$

$$1/f = 298.257 .$$

TABLE 5.7

The geoidal deflections predicted by program GDOVE.

station #	N - S comp.	stand. deviat.	E - W comp.	stand. deviat.
	"	"	"	"
1	-3.10	1.42	-3.89	1.35
2	2.20	1.42	-5.73	1.37
3	2.06	1.41	-3.41	1.35
4	-2.41	1.38	-2.99	1.36
5	-1.06	1.38	-1.74	1.37
6	-1.64	1.47	-2.05	1.35

All of the gravity anomalies are referred to the Geodetic Reference System 1967. These two ellipsoids are supposedly properly aligned; the transformation of the surface deflections are, thus, given by (Vaníček and Krakiwsky, 1982):

$$\begin{bmatrix} \xi' \\ \eta' \end{bmatrix} = \begin{bmatrix} \xi'_o \\ \eta'_o \end{bmatrix} - \begin{bmatrix} 0 & -\sin 2\Phi \\ 0 & 0 \end{bmatrix} \cdot \begin{bmatrix} da \\ df \end{bmatrix} + \begin{bmatrix} -\sin\phi\cos\lambda/a & -\sin\phi\sin\lambda/a & \cos\phi/a \\ -\sin\lambda/a & \cos\lambda/a & 0 \end{bmatrix} \cdot \begin{bmatrix} dX_o \\ dY_o \\ dZ_o \end{bmatrix} , \tag{5.1}$$

where ξ'_o, η'_o are the surface deflections refered to the original ellipsoid (a=6378135 m ,1/f=298.257),

da, df are the differences in the size and shape of the ellipsoids (The parameters of GRS67 minus those of the original ellipsoid), and

dX_o, dY_o, and dZ_o are the differences of the coordinates of the ellipsoid center with respect to the center of mass of the earth (The coordinates of GRS67 minus those of the original). Here $dX_o = dY_o = dZ_o = 0$.

In estimating the accuracy of the astro-gravimetric curvature effect, there are two different kinds of errors distinguished:

(1) error in the geoidal deflection.

(2) error in the surface deflection.

The error in the geoidal deflection has been already shown in Table 5.7.

The error in the surface deflection stems from the errors of the astronomic coordinates and the geodetic coordinates. Considering the astronomic coordinates, the inherent errors have been estimated at 0".5 in latitude and 0".6 in longitude (Rice, 1962). The systematic differences between the star catalogues used are not expected to affect the astronomic positions by more than 0".3 (Vaníček and Merry, personal communication with G.Corcoran in 1972) While the neglected reduction of the coordinates to the mean pole of 1900-1905 (Conventional International Origin) never affects more than 0".4 in latitude (Mueller, 1969). The effect on longitude can reach larger values. The distance

between the instantaneous pole and the mean pole of 1900-1905 is typically 0".2. For points in Northern Canada ($\Phi > 60^{\circ}$), the correction could be of the order of 0".5 to 1".0 (Vaníček and Merry, 1973).

Considering the geodetic coordinates, the errors are caused by three major effects: the propagation of the observational errors from the initial point of the geodetic network, the non-rigorous method of adjustment initially used in the geodetic networks, and the incomplete reduction of the observations used in the original adjustment.

An approximate formula for estimating the propagation of the observational errors from the geodetic network has been suggested by Simmons(1950):

$$\text{Proportional accuracy} \doteq M^{1/3}/20000 \ , \qquad (5.2)$$

where M is the distance in miles from the origin of the network. An estimate for the standard deviation in arcseconds is (Merry, 1975):

$$\sigma_m = 1".89 \times 10^{-5} \cdot K^{2/3} \ , \qquad (5.3)$$

where K is the distance in Kilometres from the origin of the network.

Due to the initially used non-rigorous adjustment technique, the misclosures of up to 36m in Canada (approximately 1") have been reported (Dept. of Energy, Mines and Resources, 1972). In addition, due solely to the adjustment constraints in New Brunswick, the relative errors

of 0".2 in the horizontal position have been found (Krakiwsky and Konecny, 1971).

The effect of the incomplete reduction of the observations (without considering the horizontal angles) has been estimated and does not exceed 0".5 in Canada (Merry and Vaníček, 1973).

On the basis of the above analysis of accuracy, the errors of the astro-gravimetric curvature effect can be estimated by:

$$\sigma_{\Delta\xi}{}_{A-G} = \sqrt{(\sigma_g^2 + \sigma_o^2 + \sigma_s^2 + \sigma_p^2 + \sigma_m^2 + \sigma_n^2 + \sigma_r^2)}$$
$$\sigma_{\Delta\eta}{}_{A-G} = \sqrt{(\sigma_g^2 + \sigma_o^2 + \sigma_s^2 + \sigma_p^2 + \sigma_m^2 + \sigma_n^2 + \sigma_r^2)}, \quad (5.4)$$

where σ_g is the error of the geoidal deflection, σ_o is the observational error - 0".5 in latitude and 0".6 in longitude, σ_s is the error due to the star catalogues - assumed to be 0".3, σ_p is the error due to the polar motion - 0".2 for latitude and 0".2$\tan\Phi$ for longitude, σ_m is given by equation (5.3), σ_n is the error due to the non-rigorous adjustment, and σ_r is the error due to the incomplete reduction to the ellipsoid. The total errors of σ_n and σ_r are here assumed to amount to 0".5. The astro-gravimetric curvatures and their standard deviations for the six NB points are shown in Table 4.8.

Comparisons between the astro-gravimetric (A-G) and the Stokes-Molodenskij (S-M) curvature effects are presented in Table 5.9. The standard deviations of the differences, also shown in Table 5.9, are given by:

TABLE 5.8

The astro-gravimetric curvature effect (the difference between the geoidal deflection and the surface deflection).

St. #	north-south comp.				east-west comp.			
	geoid.	surf.	A-G	σ_{A-G}	geoid.	surf.	A-G	σ_{A-G}
	"	"	"	"	"	"	"	"
1	-3.10	-1.53	-1.57	1.67	-3.89	-4.02	0.13	1.65
2	2.20	0.27	1.93	1.67	-5.73	-8.38	2.65	1.66
3	2.06	0.91	1.15	1.63	-3.41	-4.16	0.75	1.65
4	-2.41	-2.50	0.09	1.67	-2.99	-3.09	0.10	1.65
5	-1.06	-0.74	-0.32	1.64	-1.74	-2.24	0.50	1.66
6	-1.64	-2.42	0.78	1.71	-2.05	-1.30	-0.75	1.64

$$\sigma_{\delta\Delta\xi} = \sqrt{(\sigma^2_{\Delta\xi_{A-G}} + \sigma^2_{\Delta\xi_{S-M}})}$$
$$\sigma_{\delta\Delta\eta} = \sqrt{(\sigma^2_{\Delta\eta_{A-G}} + \sigma^2_{\Delta\eta_{S-M}})}. \qquad (5.5)$$

As can be seen from the results presented in Tables 5.1 through 5.8, the curvature effects of the plumb line determined by the Stokes-Molodenskij formula are much more accurate than those by the astro-gravimetric model. The standard deviations of the differences between A-G and S-M are, therefore, almost equal to those of A-G. The only value affected by σ_{S-M} is the standard deviation of the east-west component at station 2. The differences between S-M and A-G are smaller than the standard deviations of the

TABLE 5.9

Comparisons between the astro-gravimetric (A-G) and the Stokes-Molodenskij (S-M) curvature effects.

#	north-south comp.				east-west comp.			
	A-G	S-M	diff.	$\sigma_{\delta\Delta\xi}$	A-G	S-M	diff.	$\sigma_{\delta\Delta\eta}$
	"	"	"	"	"	"	"	"
1	-1.57	-0.06	-1.51	1.67	0.13	0.03	0.10	1.65
2	1.93	1.35	0.58	1.67	2.65	1.70	0.95	1.69
3	1.15	1.10	0.05	1.63	0.75	0.18	0.57	1.65
4	0.09	-0.08	0.17	1.67	0.10	0.04	0.06	1.65
5	-0.32	-0.03	-0.29	1.64	0.50	-0.01	0.51	1.66
6	0.78	0.08	0.70	1.71	-0.75	-0.03	-0.72	1.64

astro-gravimetric curvature effect. The results indicate that the Stokes-Molodenskij curvature effects are consistent with the astro-gravimetric curvature effects. In addition, the astro-gravimetric model is uneconomical and time-consuming.

CHAPTER 6

CONCLUSIONS AND RECOMMENDATIONS

Due to the uneven density distribution of the earth, the plumb lines are bent and twisted. The curvature and torsion are different from point to point and are very localized. The effects are larger in mountainous areas than in flat areas.

Some approaches for estimating the curvature effect of the plumb line have been formulated and tested. If we use the method based on the gravity field model, then the density distribution has to be well-known. If we use the method based on the relation between the curvature effect and the orthometric height correction, then a dense gravity net around the computation point is needed. The need for accurate knowledge of the crustal densties is self-evident in using the method based on density modelling. Thus good accuracies for the curvature effect of the plumb line from those methods cannot be expected (Ndyetabula, 1974). If we utilize Vening Meinesz's and Molodenskij's formulae, it becomes laborious and time-consuming to calculate the geoidal and Molodenskij's deflections separately in order to determine the plumb line curvature effect.

The objectives of the work undertaken for this thesis were to practically test another approach for the evaluation of the plumb line curvature effect. The method, developed by Vaníček and Krakiwsky (1982), is based on the combination of Stokes's and Molodenskij's approaches. From the results shown in the last chapter, the Stokes-Molodenskij curvature effects are consistent with the astro-gravimetrically determined curvature effects, but our method gives a much higher accuracy. In addition, it is easy to apply. The determination of the curvature effect of the plumb line is no longer a difficult work.

The analyses in Chapter 4 show that the contribution of the difference between the free-air anomalies on the geoid and those on the earth's surface is very small. It can be neglected without loss of accuracy. The curvature of the plumb line is mainly affected by the surrounding topography to a spherical distance of $< \text{about } 13'$ (approximately 24 km).

The Tables in last chapter demonstrate that the terrain profile effects (point effects) along the north-south and east-west directions are usually more significant than the regional terrain and gravity effects. In other words, the local terrain contributions dominate the phenomenon. Therefore, the slopes of the terrain have to be accounted for very carefully.

In this work, the method based on the combination of Stokes's and Molodenskij's approaches is first tested to determine the curvature effect of the plumb line. A formula which combines the geoidal and Molodenskij's deflections of the vertical is called the Stokes-Molodenskij formula. A contribution is also made in the development of an algorithm for numerical evaluation of the Stokes-Molodenskij formula. Another contribution is made by formulating an algorithm for terrain slope evaluation.

Since the curvature effect of the plumb line is position-dependent and since the variation from point to point is large in mountainous areas, it is difficult to predict the plumb line curvature effect from the point plumb line curvatures already known. Tables 5.1 through 5.6 show that the contribution of the regional terrain and gravity effect is at most about 0".1 in New Brunswick and seems smooth. For further studies, it is recommended that the curvature effect of the plumb line may be computed for other points in Canada. If the contributions of the regional terrain and gravity effect are smooth, then it is also recommended that the prediction of the plumb line curvature effect may be done in two steps. First, use available data for the contribution of the regional terrain and gravity effect to predict the contribution of unknown point. Secondly, determine from the topographic maps or field works the local terrain contribution.

Appendix I

THE LEAST-SQUARES APPROXIMATION

The problem of approximation can be defined as follows: given a function F, find another function of a prescribed general form to represent the given function F in a specified way (Vaníček and Wells, 1972). The given function can be represented by a generalized polynomial:

$$P(t) = \sum_{i=1}^{n} a_i \cdot Q_i(t) \quad , \qquad (I.1)$$

where a_i are the coefficients of the polynomial,

n is the number of coefficients, and

$Q_i(t)$ are the prescribed functions: they may be functions of one, two or m variables.

Provided that the prescribed functions are linearly independent of one another, they are called base functions. If and only if $Q \equiv \{Q_1, Q_2, \ldots, Q_n\}$ is a base, the least-squares determination of the coefficients of the polynomial is unique.

Let f be the given function (The functional values f are the Bouguer anomalies in section 4.2, and the tangents of the terrain inclination in section 4.6 respectively). After the base functions are selected, the coefficients are determined from the least-squares procedure (ibid., p.21):

$$\sum_{k=1}^{n} \langle Q_j , Q_k \rangle \cdot a_k = \langle f, Q_j \rangle \quad , \; j=1,2,\ldots,n \quad , \tag{I.2}$$

where the scalar products $\langle Q_j , Q_k \rangle$ and $\langle f, Q_j \rangle$ are defined by:

$$\begin{aligned} \langle Q_j , Q_k \rangle &= \sum_{i=1}^{m} W_i \cdot Q_j(t_i) \cdot Q_k(t_i) \\ \langle f , Q_j \rangle &= \sum_{i=1}^{m} W_i \cdot f(t_i) \cdot Q_j(t_i) \; , \end{aligned} \tag{I.3}$$

and m is the number of data points (functional values of f) used,

W_i is the weight function, and

$f(t_i)$ is the i-th functional value.

Equation (I.2) can be written as a matrix form:

$$\underline{G} \cdot \underline{a} = \underline{L} \; . \tag{I.4}$$

Then, the coefficients of the polynomial are determined from:

$$\underline{a} = \underline{G}^{-1} \cdot \underline{L} \; , \tag{I.5}$$

where G exists if and only if Q is a base function. After the coefficients are obtained, residuals can be computed from the observed data f_i and the estimated $P(t_i)$, given by (I.1):

$$V_i = f_i - P(t_i) \qquad i=1,2,\ldots,m \tag{I.6}$$

The variance factor σ_o^2 is then determined from:

$$\sigma_o^2 = \frac{\langle V, V \rangle}{m - n} \tag{I.7}$$

and the covariance matrix of the coefficients is:

$$\underline{C}_a = \sigma_o^2 \cdot \underline{G}^{-1}. \tag{I.8}$$

According to the law of propagation of covariance, the variance of the predicted value P(t) at any point t computed from (I.1) is given by:

$$\sigma_p^2 = \underline{Q} \cdot \underline{C}_a \cdot \underline{Q}^T. \tag{I.9}$$

Appendix II

DERIVATION OF EXPRESSION FOR MEAN GRAVITY ANOMALY

The mean gravity anomaly $\overline{\Delta g}$ is given by:

$$\overline{\Delta g} = \frac{1}{A}\iint_A \Delta g \cdot dA \ . \qquad \text{(II.1)}$$

In a local cartesian coordinate system whose origin is at an arbitrary point, if the coordinates of the midpoint of the i-th block are (X_i, Y_i), and those of the four corners of the block are (X_i+r, Y_i+s), (X_i-r, Y_i+s), (X_i+r, Y_i-s), and (X_i-r, Y_i-s), then

$$\Delta g = \frac{1}{4rs}\int_{X_i-r}^{X_i+r}\int_{Y_i-s}^{Y_i+s} \Delta g \cdot dX \cdot dY \ , \qquad \text{(II.2)}$$

where r,s are halves of the north-south and the east-west extents, repectively. The anomaly Δg is approximate by $\widetilde{\Delta g}$:

$$\widetilde{\Delta g}(X,Y) = \sum_{j,k=o}^{2} a_{jk} \cdot X^j \cdot Y^k \ . \qquad \text{(II.3)}$$

Hence, in its fully expanded form, (II.2) may be written as:

$$\overline{\Delta g} = \frac{1}{4rs} \int_{X_i - r}^{X_i + r} \int_{Y_i - s}^{Y_i + s} (a_{00} + a_{01} \cdot Y + a_{02} \cdot Y^2 + a_{10} \cdot X + a_{11} \cdot X \cdot Y + a_{12} \cdot X \cdot Y^2 + a_{20} \cdot X^2 + a_{21} \cdot X^2 \cdot Y + a_{22} \cdot X^2 \cdot Y^2) dX \cdot dY \quad . \qquad (II.4)$$

Evaluating each of the integrals in (II.4) yields

$$\overline{\Delta g} = \frac{1}{4rs} \left(a_{00} \cdot XY + \frac{a_{01}}{2} \cdot XY^2 + \frac{a_{02}}{3} \cdot XY^3 + \frac{a_{10}}{2} \cdot X^2 Y + \frac{a_{11}}{4} \cdot X^2 Y^2 + \frac{a_{12}}{6} \cdot X^2 Y^3 + \frac{a_{20}}{3} \cdot X^3 Y + \frac{a_{21}}{6} \cdot X^3 Y^2 + \frac{a_{22}}{9} \cdot X^3 Y^3 \right) \Bigg|_{X = X_i - r}^{X_i + r} \Bigg|_{Y = Y_i - s}^{Y_i + s} \qquad (II.5)$$

and the mean gravity anomaly $\overline{\Delta g}$ is given by:

$$\overline{\Delta g} = a_{00} + a_{01} \cdot Y_i + a_{02} \cdot \left(Y_i^2 + \frac{s^2}{3} \right) + a_{10} \cdot X_i + a_{11} \cdot X_i \cdot Y_i + a_{12} \cdot \left(X_i \cdot Y_i^2 + \frac{X_i \cdot s^2}{3} \right) + a_{20} \cdot \left(X_i^2 + \frac{r^2}{3} \right) + a_{21} \cdot \left(X_i^2 \cdot Y_i + \frac{Y_i \cdot r^2}{3} \right) + a_{22} \cdot \left(X_i^2 \cdot Y_i^2 + \frac{X_i^2 \cdot s^2}{3} + \frac{Y_i^2 \cdot r^2}{3} + \frac{r^2 \cdot s^2}{9} \right) \quad , \qquad (II.6)$$

or, it may be written as:

$$\overline{\Delta g} = \Delta g(X_i, Y_i) + a_{02} \cdot \frac{s^2}{3} + a_{12} \cdot \frac{X_i \cdot s^2}{3} + a_{20} \cdot \frac{r^2}{3} + a_{21} \cdot \frac{Y_i \cdot r^2}{3} + a_{22} \cdot \left(\frac{X_i^2 \cdot s^2}{3} + \frac{Y_i^2 \cdot r^2}{3} + \frac{r^2 \cdot s^2}{9} \right) \qquad (II.7)$$

If the origin (X_o, Y_o) is selected to coincide with (X_i, Y_i), then equation (II.7) becomes:

$$\overline{\Delta g} = a_{00} + a_{02} \cdot \frac{s^2}{3} + a_{20} \cdot \frac{r^2}{3} + a_{22} \cdot \frac{r^2 \cdot s^2}{9} \quad . \qquad \text{(II.8)}$$

Appendix III

DERIVATION OF THE CENTRAL BLOCK CONTRIBUTION

The contribution of the central block is:

$$\Delta\xi_{1,2} = \frac{1}{2\pi\gamma_m}\iint_{A_2}\Delta G\cdot\frac{\cos\alpha}{s}\cdot ds\cdot d\alpha$$
$$\Delta\eta_{1,2} = \frac{1}{2\pi\gamma_m}\iint_{A_2}\Delta G\cdot\frac{\sin\alpha}{s}\cdot ds\cdot d\alpha \qquad \text{(III.1)}$$

and

$$\Delta G = \frac{1}{2\pi}\iint_{\Delta A_2}\frac{H-H_p}{s^2}\cdot\widetilde{\Delta g}\cdot ds\cdot d\alpha\ , \qquad \text{(III.2)}$$

where A_2 is the area of the central block and ΔA_2 is the the area of the circular ring compartment.

If the values of $\widetilde{\Delta g}$ and H are replaced by the mean values of $\overline{\Delta g}$ and $\overline{H}$ for the compartment, equations (III.1) and (III.2) become

$$\Delta\xi_{1,2} = \frac{1}{2\pi\gamma_m}\sum_{i=1}^{m}\int_{\alpha_1}^{\alpha_2}\int_{S_1}^{S_2}\Delta G_i\cdot\frac{\cos\alpha}{s}\cdot ds\cdot d\alpha$$
$$\Delta\eta_{1,2} = \frac{1}{2\pi\gamma_m}\sum_{i=1}^{m}\int_{\alpha_1}^{\alpha_2}\int_{S_1}^{S_2}\Delta G_i\cdot\frac{\sin\alpha}{s}\cdot ds\cdot d\alpha \qquad \text{(III.3)}$$

and

$$\Delta G_i = \frac{1}{2\pi}\int_{\alpha_1}^{\alpha_2}\int_{S_1}^{S_2}\frac{\overline{H}_i-H_p}{s^2}\cdot\overline{\Delta g}_i\cdot ds\cdot d\alpha\ , \qquad \text{(III.4)}$$

where m is the number of the compartments used,

α_1, α_2 are the boundaries of the compartment for azimuth,

s_1, s_2 are the boundaries for distance,

$\bar{H}_i$ is the mean height of the compartment, and

$\overline{\Delta g}_i$ is the mean free-air anomaly.

Integrating (III.1) and (III.2) over s, we obtain

$$\Delta\Xi_{1,2} = \frac{1}{2\pi\gamma_m}\sum_{i=1}^{m}\int_{\alpha_1}^{\alpha_2}\Delta G_i\cdot\cos\alpha\cdot\ln(s_2/s_1)\cdot d\alpha$$
$$\Delta\Upsilon_{1,2} = \frac{1}{2\pi\gamma_m}\sum_{i=1}^{m}\int_{\alpha_1}^{\alpha_2}\Delta G_i\cdot\sin\alpha\cdot\ln(s_2/s_1)\cdot d\alpha \qquad \text{(III.5)}$$

and

$$\Delta G_i = \frac{1}{2\pi}\int_{\alpha_1}^{\alpha_2}(\bar{H}_i - H_p)\cdot\overline{\Delta g}_i\cdot\left(\frac{1}{s_1}-\frac{1}{s_2}\right)\cdot d\alpha\ . \qquad \text{(III.6)}$$

Performing the integration over α, the contribution of the central block is given by:

$$\Delta\Xi = \frac{1}{2\pi\gamma_m}\sum_{i=1}^{m}\Delta G_i\cdot(\sin\alpha_2-\sin\alpha_1)\cdot\ln(s_2/s_1)$$
$$\Delta\Upsilon = \frac{1}{2\pi\gamma_m}\sum_{i=1}^{m}\Delta G_i\cdot(\cos\alpha_1-\cos\alpha_2)\cdot\ln(s_2/s_1) \qquad \text{(III.7)}$$

and

$$\Delta G_i = \frac{1}{2\pi}\cdot(\alpha_2-\alpha_1)\cdot(\bar{H}_i - H_p)\cdot\overline{\Delta g}_i\cdot\left(\frac{1}{s_1}-\frac{1}{s_2}\right)\ . \qquad \text{(III.8)}$$

REFERENCES

Arnold, K. (1960). Numerische Beispiele zur strengen Theorie der Figur der Erde, Veroff. Inst. Postsdam, Neue Serie Nr.16, Germany.

Arnold, K. (1962a). Gravimetric Deflections of the Vertical in High Mountains Determined by Free—Air Anomalies, Bull. Geod., No. 63, pp. 73—74.

Arnold, K. (1962b). Recent Achievement in the Theory of the LevelSurfaces of the Earth, Bull. Geod., No. 63, pp. 39—42.

Bomford, G. (1971). Geodesy, Third Edition, Oxford University Press.

Derenyi, E.E. (1965). Deflections of the Vertical in Central New Brunswick, M.Sc.E. Thesis, Department of Surveying Engineering, University of New Brunswick.

Faucher, F. (1984). Personal Communication, Surveys and Mapping Branch, Geodetic Survey of Canada.

Graaff—Hunter, J.DE. and G. Bomford (1928), Geod. Ref. Surv. India 5, pp. 118—128.

Groten, E. (1981). Determination of the Plumb Line Curvature by Astronomical and Gravimetric Methods, NOAA Technical Memorandum, NOS NGS—30.

Gysen, H.V. (1980). Precise Gravimetric Deflections of the Vertical in the Canberra Area, Australian J. Geod. Photo. Surv., No. 32, pp. 1—43.

Heiskanen, W.A. and F.A. Vening Meinesz (1958). The Earth and Its Gravity Field, McGraw—Hill Book Co., Inc., New York.

Heiskanen, W.A. and H. Moritz (1967). Physical Geodesy, W.H. Freeman San Francisco.

Helmert, F.R. (1880). Die Mathematischen und Physikalischen Theorien der Hoheren Geodasie, Vol. 2 Leipzig.

Kassim, F.A. (1980). An Evaluation of Three Techniques for the Prediction of Gravity Anomalies in Canada, Technical Report No. 73, Department of Surveying Engineering, University of New Brunswick.

Kobold, F. and E. Hunziker (1962). Communication sur la Courbure de la Vertical. Bull. Geod., No. 65, pp. 265–267.

Krakiwsky, E.J. and G. Konecny (1971). Analysis of the Primary and Secondary Control, The Canadian Surveyor, Vol. 25, No. 2, pp. 144–155.

Lachapelle, G. and K.P. Schwarz (1980). Empirical Determination of the Gravity Anomaly Covariance Function in Mountainous Areas, The Canadian Surveyor, Vol. 34, No. 3, pp. 251–264.

Ledersteger, K. (1955). Die Reduction der Astronomichen Beobachtungen Wegen Lokkrummung, Schweizerische Weitscrift fur Vermessung, and Kulturtechnik and Photogrammetrie.

Merry, C.L. (1975). Studies towards An Astrogravimetric Geoid for Canada, Technical Report No.31, Department of Surveying Engineering, University of New Brunswick.

Merry, C.L. (1980). A Practical Comparison of Some Methods of Prediction Point Gravity Anomalies, Manuscripta Geodaetica, Vol. 5, pp. 299–314.

Merry, C.L. and P. Vaníček (1973). Horizontal Control and the Geoid in Canada, The Canadian Surveyor, Vol. 27, No. 1, pp. 23–31.

Molodenskij, M.S., V.F. Eremeev, and M.I. Yurkina (1962). Methods for Study of the External Gravitational Field and Figure of the Earth, Translation from Russian (1960). Jerusalem, Israel Program for Scientific Translations.

Moritz, H. (1980a). Geodetic Reference System 1980, Bull. Geod., No. 65, pp. 395–405.

Moritz, H. (1980b). Advanced Physical Geodesy, Herbert Wichmann.

Mueller, I.I. (1969). Spherical and Practical Astronomy as Applied to Geodesy, F. Ungar, New York.

Ndyetabula, S.L.P. (1974). A Study on the Curvature of the Lines of Force of Gravity, M.Sc.E. Thesis, Department of Surveying Engineering, University of New Brunswick.

Rapp, H.R. (1981). The Earth's Gravity Field to Degree and Order 180 Using SEASAT Altimeter Data, Terrestrial Gravity Data, and Other Data, Report No. 322, Department of Geodetic Science, Ohio State University.

Rice, D.A. (1952). Deflections of the Vertical from Gravity Anomalies, Bull. Geod., No. 25, pp. 285–312.

Rice, D.A. (1962). A Geoidal Section in the United States, Bull. Geod., No. 65, pp. 243–251.

Rizos, C. (1982). The Role of the Geoid in High Precision Geodesy and Oceanography, Deutsche Geodatische Kommission.

Sünkel, H. and G. Kraiger (1983). The Prediction of Free–Air Anomalies, Manuscripta Geodaetica, Vol. 8, pp. 229–248.

Vaníček, P. (1974). Brief Outline of The Molodenskij Theory, Lecture Notes No. 23, Department of Surveying Engineering, University of New Brunswick.

Vaníček, P. (1980). Introduction to Adjustment Calculus, Third Edition,Lecture Notes No. 35, Department of Surveying Engineering, University of New Brunswick.

Vaníček, P. and C.L. Merry (1973). Determination of the Geoid from Deflections of the Vertical Using A Least–Squares Surface Fitting Technique. Bull. Geod., No. 109, pp. 261–279.

Vaníček, P. and D. Christodulides (1974). A Method for the Evaluation of Vertical Crustal Movements from Scattered Geodetic Relevellings, Canadian Journal of Earth Sciences 11(5), pp. 605–610.

Vaníček, P. and D.E. Wells (1972). The Least–Squares Approximation and Related Topics, Lecture Notes No. 22, Department of Surveying Engineering, University of New Brunswick.

Vaníček, P. and E.J. Krakiwsky (1982). Geodesy: The Concept, North–Holland Publishing Company, Amsterdam.

Torge, W. (1980). Geodesy, Walter de Gruyter & Co., Berlin.

Zakatov, P.S. (1962). A Course in Higher Geodesy, The National Science Foundation, Washington, D.C.